Construction and Building Materials 529 (2026) 146571

Contents lists available at ScienceDirect

Construction and Building Materials

journal homepage: www.elsevier.com/locate/conbuildmat

Experimental and numerical investigation of a cement-stabilized compressed earth block masonry system

Jacopo Baldelli [a,*], Giosuè Boscato [b], Makhaly Ba [c], Antonella Cecchi [a]

[a] Università Iuav di Venezia, Venice, Italy
[b] Department of Structural and Geotechnical Engineering, Sapienza Università di Roma, Rome, Italy
[c] Department of Geotechnics, UFR Sciences de l'Ingénieur, Université Iba Der Thiam de Thiès, Thiès, Senegal

ARTICLE INFO

Keywords:
Stabilized Compressed Earth Block (SCEB)
Earth-based mortar
Earthen masonry
Homogenization
Non-linear numerical analysis

ABSTRACT

Compressed earth block (CEB) masonry represents a sustainable construction technique aligned with environmentally and socially responsible building practices. This study investigates the mechanical behavior of an unreinforced cement-stabilized compressed earth block (SCEB) masonry system currently under development in Senegal, using locally sourced soil from the Sindia region for both block and mortar production. The mechanical properties of the system are evaluated at the unit-scale, with particular attention to the influence of specimen geometry and moisture conditions. At the meso-scale, masonry panels are tested under uniaxial compression to investigate load-bearing capacity, deformation behavior, crack development, and failure mechanisms. Experimental results highlight the role of block geometry and material heterogeneity in governing the mechanical response of masonry. A data-efficient numerical model is proposed and calibrated against the experimental results. The model captures the primary mechanical response of unreinforced SCEB masonry while requiring a limited set of input parameters, making it suitable for applications where material variability and limited experimental data challenge conventional modeling approaches. The results contribute to a more systematic understanding of stabilized compressed earth block masonry and provide a methodological basis for its mechanical assessment and future optimization for structural applications.

1. Introduction

Affordable housing has been in growing demand, particularly in low- to middle-income contexts [1,2], prompting renewed interest in construction materials and techniques which allow for a reduced environmental impact [3,4], while remaining socially and economically viable. In a broader sense, as adopted by international frameworks, sustainability encompasses environmental performance, economic accessibility, and social equity [5], dimensions that are particularly relevant within the building sector. In many regions, particularly in the Global South, access to industrialized materials such as fired bricks or reinforced concrete remains constrained by cost, availability, and supply-chain barriers, which can contribute to limitations in their adoption within affordable housing programs [6,7]. In this context, earthen construction techniques such as adobe, rammed earth, and compressed earth blocks (CEBs) may offer a more sustainable option for construction applications, as they rely on locally available resources (soil) [8–11], require lower embodied energy and environmental footprint [3,8,9,12,13], and exhibit enhanced thermal behavior and indoor comfort [14–16], making them an appealing solution for environmentally and economically sustainable housing.

Among earthen technologies, compressed earth blocks have increasingly been adopted as a technically refined reinterpretation of traditional sun-dried earth blocks (adobe) [9,17], proposing a semi-artisanal approach to earth building with improved performance and reproducibility. They combine the environmental sustainability and local adaptability of earthen constructions with the modularity and construction efficiency of masonry, allowing for scalable implementation through simple, low-energy manufacturing techniques [18–22]. The CEB system offers a technically reliable yet economically accessible solution for housing, consistent with the goals of sustainable construction. Beyond material efficiency, the low-tech and semi-artisanal process enables in situ fabrication, adopting simple equipment, without requiring highly specialized labor. This aspect enhances replicability in resource-limited contexts, reinforcing both social and economic dimensions of sustainability.

* Corresponding author.
E-mail address: jbaldelli@iuav.it (J. Baldelli).

https://doi.org/10.1016/j.conbuildmat.2026.146571
Received 9 February 2026; Received in revised form 15 April 2026; Accepted 30 April 2026
Available online 6 May 2026
0950-0618/© 2026 The Authors. Published by Elsevier Ltd. This is an open access article under the CC BY license (http://creativecommons.org/licenses/by/4.0/).

Raw earth, in its natural state, lacks mechanical strength and durability required for structural applications when compared with conventional construction materials such as fired brick or concrete [23–26]. To achieve minimum performance levels, compatible with structural use and adequate resistance to external actions, stabilization is one widely employed solution in earthen construction [8,19,27–30]. Stabilization can be achieved through mechanical, physical or chemical alteration of the soil mix. In the case of chemical stabilization, organic or inorganic binders are added to improve cohesion among soil particles, stiffness, and long-term durability [18,31]. Common chemical stabilizers include cement, lime, and bitumen, while industrial by-products (such as fly ash or rice husk) are increasingly explored to improve the environmental compatibility of stabilized soils [32,33]. Despite its environmental impact, cement remains one of the more effective and widely adopted stabilizers for achieving structural-grade strength, dimensional stability, and water resistance in compressed earth block production and, more generally, in earthen construction techniques [25,34–40], especially when sandy soils are employed [19,41,42]. Comparatively standardized formulation and predictable behavior make cement particularly suitable for research and structural applications, where earth itself remains a highly heterogeneous material with limited regulatory and testing frameworks. For these reasons, cement stabilization continues to be employed when structural reliability and repeatability are key design considerations.

At the material scale, earthen materials exhibit intrinsic heterogeneity due to their three-phase composition comprising solid particles, water, and air, which vary according to local soil type and moisture conditions, and grain size distribution [43,44]. The use of site-sourced soils, a defining feature of earthen construction, leads to additional variability in mineralogical composition and particle grading. Combined with the often semi-artisanal production processes, the resulting material presents physical and mechanical properties which are highly dependent on local practice, locally sourced soil, and, where applicable, traditional stabilization procedure [45], and therefore it cannot yet be considered standardized. Geometrical and dimensional variability is also introduced, as shapes, dimensions, and proportions are not standardized in the CEB production. Furthermore, testing configurations for earthen materials remain diverse, with significant variation in specimen geometry and boundary conditions, which can lead to complications in cross-study comparability of mechanical data [46–49].

In this context, the present study investigates a cement-stabilized compressed earth block (SCEB) masonry assemblage, proposed as a technically reliable solution for affordable housing, evaluating its mechanical suitability under quasi-static compressive loading through a combined experimental and numerical approach. The work is part of a broader research program investigating the influence of different reinforcement strategies at the meso-scale. It should be noted that the characterization of the constituent materials and the unreinforced earth masonry panels was carried out to estimate the mechanical properties of the artisanal materials adopted, rather than to optimize their composition. Within this framework, the methodology envisages the following steps:

- characterization of the constituent materials, blocks and mortar, to estimate their mechanical properties rather than to optimize their composition.
- experimental testing of masonry assemblages under compressive loading to evaluate the response of the system at the meso-scale.
- development of a homogenized finite element model comprising two steps: (i) a micro-scale homogenization procedure based on the experimentally determined constituent material properties, and (ii) a macro-scale model adopting the homogenized properties to reproduce the mechanical response of the masonry assemblage and investigate different modeling assumptions.

The paper is organized as follows. Section 2 describes the geometry and production of the SCEBs, and the construction system adopted for the masonry assemblages. Section 3 presents (i) the identification of the soil typology based on available literature, (ii) the mechanical characterization of earth blocks and (iii) the mechanical characterization of earth-based mortars. Section 4 reports the experimental investigation carried out on unreinforced masonry panels. Section 5 introduces the numerical modeling strategy, including the homogenization procedure and the development of preliminary linear and nonlinear models.

2. Material and geometric description of blocks and masonry

The masonry assemblage investigated in this study was developed in Senegal and consists of cement-stabilized compressed earth blocks (SCEBs) combined with an earth-based mortar.

Block fabrication, mortar production, and the overall realization of the construction system rely on a semi-artisanal process, assisted only by rudimentary equipment. The entire production process relies on operator-defined practices: raw materials are proportioned by volume using basic containers rather than by weight, and mold filling for block compaction is performed manually. These factors introduce human-induced variability in the composition and compaction of individual elements, which may affect mechanical response. Such variability is not considered a limitation of the present study but rather an inherent characteristic of the investigated system, representative of real construction practice in the target context. The construction system includes a reinforced frame (steel–concrete frame) integrated within the masonry; in the present study, however, only the unreinforced configuration was analyzed to isolate the mechanical response of the earth-based components. The dry mix used for the SCEBs consisted of sieved red earth, fine sand, and cement in a 10:2:1 ratio, expressed in approximate volumetric terms based on common on-site batching practices (e.g., buckets or wheelbarrows). The earth used for block production was described by the manufacturer as “sieved”, with no specification of the sieve size (see Section 3.1 for the adopted soil composition). Water was added to achieve the desired consistency, corresponding to approximately 10% by volume of the dry constituents. The workability of the mixture was adjusted to obtain a slightly damp and friable consistency suitable for compaction, and the adequacy of the moisture content was verified through manual handling, whereby the mixture formed a cohesive lump when compressed by hand without exhibiting plastic deformation or sticking [8]. This value is consistent with the molding moisture contents commonly reported for compressed earth block production under static compaction, typically ranging between 10% and 13% [50]. The adopted moisture condition is also consistent with the concept of optimum moisture content governing soil compaction behavior [19].

Blocks were produced using a hydraulic press with geometric stops: a fixed volume of wet earth mix was manually poured into a mold (up to 150 mm) and compressed to a final height of 90 mm under an average pressure of 3 MPa, with compaction (F_c) applied along the x_2 direction (Fig. 1a). Although this method ensures dimensional consistency, variations in the introduced volume can affect the physical and mechanical properties of the blocks, requiring careful quality control. The geometry of the cement-stabilized compressed earth blocks (SCEBs) adopted in this study is shown in (Fig. 1b). Two block typologies were produced, differing in the arrangement of cylindrical voids designed to accommodate vertical reinforcement while preserving alignment with the header-masonry bond (Fig. 1c). In the following, these two configurations are referred to as Block-1 and Block-2, respectively.

A Cartesian reference system x_1, x_2, x_3 is adopted throughout the study, as shown in Fig. 1, with x_2 aligned with the compaction and loading direction, and corresponding to the block height, x_1 corresponding to the block width, and x_3 to the thickness of the masonry wall t_M which corresponds to the block length.

Given the variability of natural earthen materials, the geotechnical properties of the locally sourced lateritic soils were considered to verify

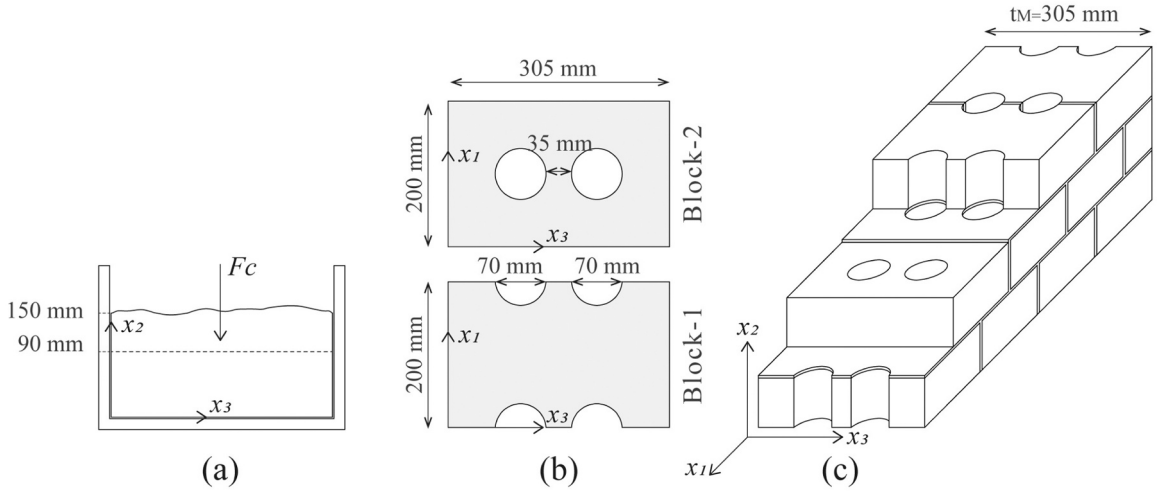


Fig. 1. Cement-stabilized Compressed Earth Block: (a) compaction procedure, (b) block typologies and (c) masonry bond configuration.

their suitability for cement stabilization prior to the investigation of mechanical behavior.

3. Experimental campaign on constituent materials

The experimental campaign was designed to characterize the constituent materials of the masonry assemblage at different scales. The investigation addressed the suitability of the locally sourced soils for cement stabilization, based on a previous geotechnical and chemical study by Diop et al. [51], the mechanical properties of the SCEBS, and of the earth-based mortar. Hereafter mean values are denoted by $\langle \bullet \rangle$.

3.1. Soil investigation

In the present study, the soil characterization is referenced to Diop et al. [51], as the material was sourced from the same site (Ngaparou, locality of Thiès region, Senegal). According to [51], two lateritic soil samples from the same site were considered, distinguished based on a 4 mm sieve criterion: one consisting of particles passing 4 mm, S-1, and the other of particles retained on 4 mm, S-2.

The geotechnical properties considered in this work refer to a mixture of these two samples, composed of 50% S-1 and 50% S-2 (M-1), as defined in [51]. This mixture can be interpreted as a balanced combination of finer and coarser fractions, representative of the grading conditions adopted for compressed earth block production. Such a combination is consistent with common practice in compressed earth block manufacturing, where a balanced particle-size distribution, combining fine particles (contributing to cohesion) and coarser fractions (providing a granular skeleton), is required to ensure adequate compaction and mechanical stability [52,53].

The chemical composition of lateritic soil from the Sindia region, reported by Diop et al. [51], is characterized by the presence of silica (SiO_2, 79.06% in S-1 and 51.8% in S-2), alumina (Al_2O_3), and iron oxide (Fe_2O_3, 10.7% in S-1 and 29.84% in S-2), which are typical constituents of lateritic materials. Variations in the relative proportions of silica, alumina, and iron oxide reflect differences between finer and coarser fractions. The low contents of lime (CaO, 0.68% in S-1 and 0.82% in S-2) and magnesia (MgO, 0.15% in S-1 and 0.11% in S-2) indicate a limited natural cementation potential, consistent with non-calcareous laterites reported in the literature [54–56]. At the same time, the relatively high silica content and moderate alumina levels are indicative of sandy to silty textures commonly regarded as compatible with cement stabilization [53,57].

Based on the particle-size distribution obtained from sieve analysis, M-1 soil consists of approximately 15.6% gravel (>2 mm), 53.3% sand (0.063–2 mm), and 31.2% fines (<0.063 mm), according to standard geotechnical size classifications. The available grading data does not allow separation of the fines fraction into silt and clay. However, the Atterberg limits (LL = 23%, PI = 11%) [51] indicate low-plasticity clayey fines, suggesting a moderate clay fraction without highly clay-rich behavior.

The mechanical data reported by Diop et al. [51] show that these soils respond positively to cement stabilization, with compressive strength increasing as a function of cement content, while no comparable improvement was observed with fly ash. Based on this evidence, cement stabilization was adopted in the present study as a suitable approach for the production of SCEB.

At the material level, and within the range of grading conditions described above, the dry mixture designed for cement-stabilized compressed earth blocks (SCEB) incorporates sand to adjust the grading and reduce the clay fraction, thereby enhancing the effectiveness of cement stabilization [57–59]. This adjustment of particle-size distributions promotes and contributes to the mechanical performance and durability of the blocks [60,61].

3.2. Mechanical characterization of cement-stabilized compressed earth blocks

In view of the limited standardization in the construction and testing of earth-based masonry elements, the mechanical response of the masonry assemblage was first investigated through an experimental campaign conducted at the level of the constituent materials, focusing on the block units and the mortar. Compression and bending tests were carried out on the earth blocks to assess their structural performance. For this purpose, both cubic and prismatic specimens were cut from the original blocks. The blocks were produced in situ and left to cure under natural sun-drying conditions for 28 days (average ambient conditions in Dakar in January 2024 were approximately 25 °C and 68% relative humidity [62]). This curing period allowed the cement stabilization process to develop the mechanical strength of the units. After curing, cubic and prismatic specimens were extracted from the original blocks for mechanical testing. The main specimen physical properties are summarized below:

- block density $\langle \rho_b \rangle = 1840 \text{kg/m}^3$, COV = 0.04;
- specimen dimensions: $90 \times 90 \times 90 \text{mm}^3 90 \times 90 \times 270 \text{mm}^3$.

3.2.1. Compression test

To determine the compressive strength f_c^b and elastic properties (i.e.,

elastic modulus E^b and Poisson ratio ν^b) of cement-stabilized compressed earth blocks (SCEB), the mechanical response under uniaxial compression, conducted under unconfined conditions, was investigated, assuming an isotropic material behavior at the specimen scale. Consistent with the lack of standardized testing procedures for earthen materials discussed in Section 1, no universally adopted compression testing protocol currently exists. Various studies adopt different specimen sizes and geometries, resulting in limited methodological consistency across the literature. A common approach involves testing full masonry units. However, the geometry of full blocks may influence the stress state during compression tests, potentially promoting the development of transverse stress components and leading to deviations from an ideal uniaxial compression condition. Alternative approaches include the use of prismatic specimens or stacked halves joined with a mortar bed. However, the introduction of a mortar layer leads to a composite mechanical response, which is not representative of the properties of the block itself [63]. Cube-shaped specimens have also been employed to mitigate confinement effects. Morel et al. [63] noted that compression tests on cubic specimens are reliable when the cubes are cut directly from the blocks, rather than molded separately. In the present study, both cubic and full block specimens were tested under uniaxial compression. The following subsections present the experimental program for each configuration, followed by the results obtained under saturated conditions.

3.2.1.1. Compression test on cubic specimens. Cubic specimens were selected as the primary configuration for mechanical characterization, as this geometry most closely aligns with standardized testing procedures commonly adopted for concrete and cement-based materials. Given that the material was stabilized with 8% cement, standardized procedures for concrete testing were considered appropriate for defining the test setup. According to UNI EN 12390–1:2021, Testing hardened concrete – Part 1: Shape, dimensions and other requirements for specimens and molds [64], specimen geometries for concrete include cubes, cylinders, and core-extracted samples. Cubic specimens are often preferred due to their ability to ensure a uniform stress distribution, thereby improving repeatability and test reliability. While some confinement effects may still occur, these are implicitly accounted for within the standardized testing framework.

The cubic specimens used in this study were cut directly from the compressed blocks, resulting in a final specimen size of $90 \times 90 \times 90\text{mm}^3$ as shown in Fig. 2. This differs from the standard dimensions prescribed by [64] (cube length of 100, 150, and 200 mm), the deviation being dictated by the block height from which the cubes were extracted (see Fig. 2b). A total of 13 specimens were tested. No friction-reducing interface was placed between the specimen faces and the loading platens, as this could have promoted lateral dilation along the x_1 direction, altering the uniaxial stress state.

Tests were performed under displacement control at a loading rate of 0.5 mm/min. Each specimen was instrumented along the x_1 and x_2 directions to evaluate the elastic modulus and Poisson ratio (see Fig. 2). Strain measurements were performed using biaxial rosette strain gauges (Micro-Epsilon PL-30–11, 120 Ω, gauge length 30 mm, bidirectional), bonded to the specimen surface using cyanoacrylate adhesive.

The cubic specimens exhibited a compressive strength of $\langle f_c^b \rangle = 5.9\text{MPa}$ (COV = 0.11) with a corresponding axial strain of $\langle \varepsilon_2^b \rangle = 0.0023$. The elastic modulus was evaluated from the tangent slope of the initial linear portion of the stress-strain curve, i.e., the interval in which stress and strain remained approximately proportional before the first evident nonlinear deviation. For compression tests on cubic specimens, the initial linear interval adopted for modulus evaluation is identified in Fig. 3b by the origin and the reference points A (-9.7×10^{-5}, 2.8 MPa) and B (-4.0×10^{-4}, 1.32 MPa). The elastic modulus was determined as $\langle E^b \rangle = 6989$ MPa (COV = 0.4). The Poisson ratio was $\langle \nu^b \rangle = 0.34$, determined as $\nu = -\varepsilon_1/\varepsilon_2$. The reported axial strain $\langle \varepsilon_2^b \rangle$ refers to the maximum value recorded during the test and coincides with specimen failure, consistent with the brittle response of the material.

Two distinct crack patterns were observed. The most frequently observed failure mode consisted of diagonal cracking across the specimen, forming an X-shaped pattern (see Fig. 4a) which is consistent with the crack configuration considered acceptable for concrete cubic specimens according to UNI EN 12390–3 [65]. In fewer cases, failure occurred through predominantly vertical cracking developing in the $x_1 - x_2$ and $x_3 - x_2$ planes, leading to progressive fracture and eventual splitting of the specimen (Fig. 4c). In these cases, no cracking was observed in the $x_1 - x_3$ plane, and the vertical cracks were distributed symmetrically with respect to the loading axis. On this basis, the observed failure mechanisms were considered compatible with the acceptance criteria prescribed by UNI standards.

3.2.1.2. Compression test on full block specimens. Full block specimens were tested to assess the influence of block geometry, specifically the presence of voids, on compressive strength. Due to the heterogeneous cross-section (shown in Fig. 1b), the block presents internal voids, resulting in a two-phase cross-section comprising compressed earth and void regions. Elastic parameters, such as elastic modulus and Poisson ratio, would reflect the combined response of the earthen material and the void geometry, rather than the intrinsic properties of the material itself. For this reason, strain instrumentation was not employed and elastic parameters were not derived. The characterization of elastic properties was therefore carried out exclusively on cubic specimens, as reported in subsection "Compression test on cubic specimens".

To assess the influence of specimen geometry on compressive

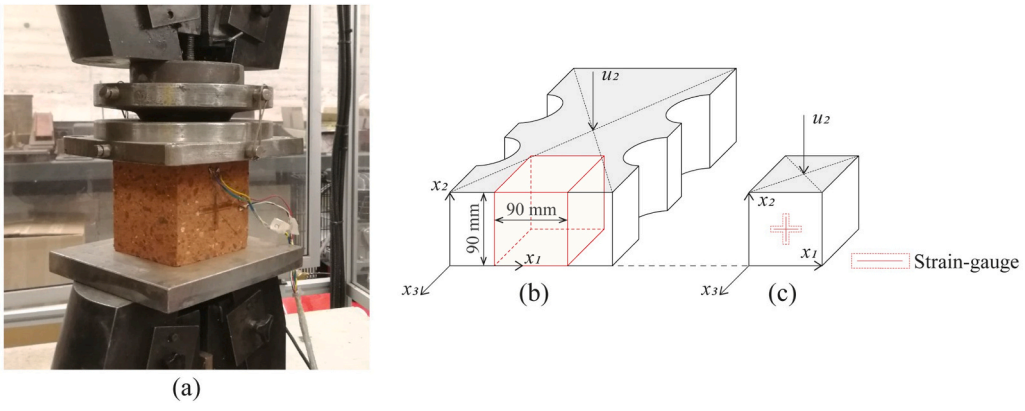


Fig. 2. Extraction of a cubic specimen from the full block and uniaxial compression test setup under unconfined conditions: (a) experimental setup; (b) full block; (c) cube specimen with strain gauge configuration.

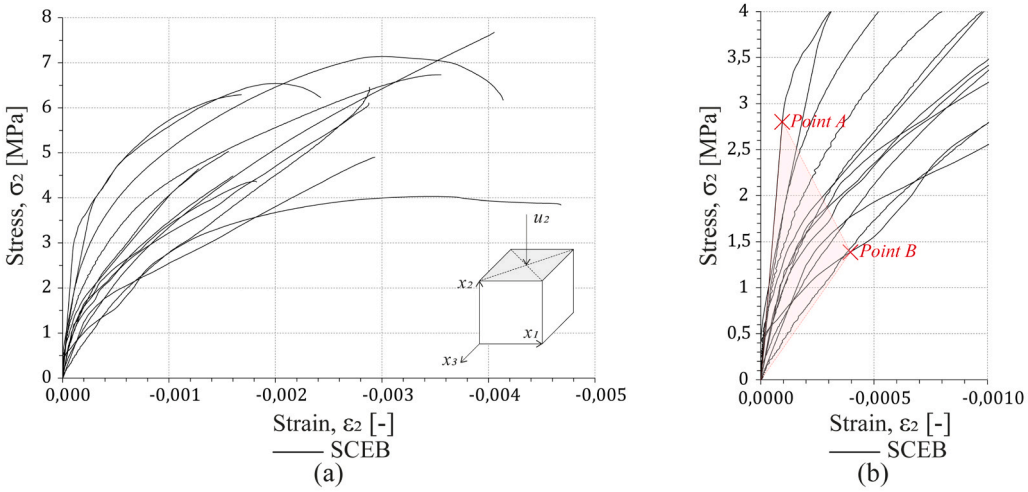


Fig. 3. (a) Stress-strain plot of cubic SCEB specimen tested in compression, x_2 direction, and (b) detail of the initial portion of the stress-strain curves.

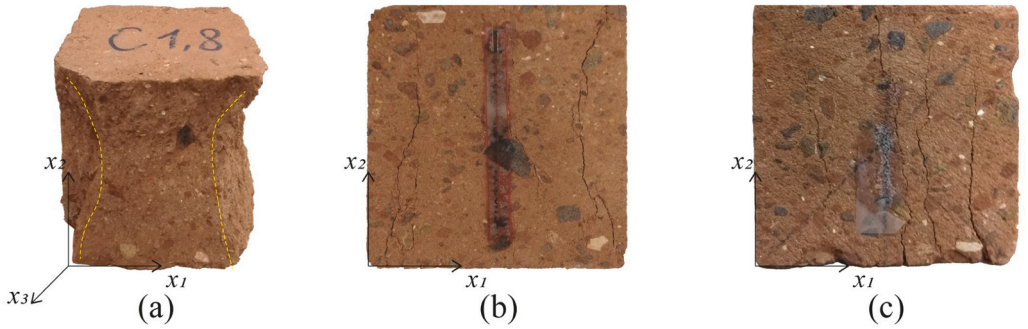


Fig. 4. Crack pattern typologies for cubic specimens, X-shaped pattern in (a) perspective and (b) frontal view, and (c) vertical cracking.

strength, six full-sized blocks from both block typologies were tested under uniaxial compression (three Block-1 and three Block-2). The same experimental setup adopted for the cubic specimens was used (see Fig. 2a).

Block-1 exhibited an average compressive strength of $\langle f_c^{FB1} \rangle$ = 8.5 MPa (COV = 0.18) and Block-2 showed $\langle f_c^{FB2} \rangle$ = 8.1 MPa (COV = 0.15). Given the limited difference between the two configurations, an average compressive strength of $\langle f_c^{FB} \rangle$ = 8.4MPa (COV = 0.17) was adopted as representative for the SCEB unit.

3.2.1.3. Compression test under saturated conditions. Since the mechanical performance of earthen-based materials is strongly influenced by moisture content, additional compression tests were performed under saturated conditions for both cubic and full block specimens. Prior to testing, specimens were submerged in water for 24 hours, in accordance with procedures commonly adopted in the literature [66,67]. Five cubic specimens and six full blocks (three Block-1 and three Block-2 specimens) were investigated. The same experimental setup adopted for the dry configuration was used.

Water absorption results for saturated specimens are reported in Table 1. Both specimen types exhibited comparable absorption levels (A_w), with average values of 13.6% for cubic specimens and 12.6% for full blocks.

Compressive strength under saturated conditions exhibited a marked reduction with respect to the dry state. For cube specimens, the mean strength decreased from 5.9 MPa to $\langle f_c^{b,s} \rangle$ = 2.8 MPa (COV = 0.14), corresponding to a retention of approximately 48%. A larger reduction was observed for SCEB units, whose mean strength dropped from 8.6 MPa to $\langle f_c^{FB,s} \rangle$ = 3.3 MPa (COV = 0.35), corresponding to about 38% of the dry value. One SCEB specimen showed a higher residual capacity (5.6 MPa, 65% retention).

Cubic specimens exhibited a conjugate diagonal cracking pattern under saturated conditions. Full block specimens failed predominantly through tensile cracking initiated at geometric discontinuities and section reductions along the loading plane, with cracking frequently observed in correspondence with the void regions (see Fig. 5).

3.2.1.4. Compressive test results and discussion. The results obtained across the different specimen configurations and moisture conditions are discussed here comparatively, with reference to the influence of specimen geometry and moisture on the measured compressive response.

Compressive strength for SCEB falls at the higher end of strength values suggested by CRAterre [68] as well as for elastic parameters (ν^b, E^b), indicating that the material meets the requirements for building construction. The relatively high variability observed for the elastic modulus (COV = 0.4) may be related to the inherent heterogeneity of the material.

In terms of compressive strength, the values obtained for cubic specimens are consistent with those reported for SCEB stabilized with comparable cement contents (≈8%) [50,69–72]. Comparable ranges are

Table 1
Dry weight (P), saturated weight (P_s), and absorbed water (A_w) for SCEB.

	$\langle P \rangle$		$\langle P_s \rangle$		$\langle A_w \rangle$	
	[g]	COV	[g]	COV	[%]	COV
Cube	1334	0.011	1515	0.012	13.6	0.034
Full block	9281	0.032	10460	0.036	12.7	0.042

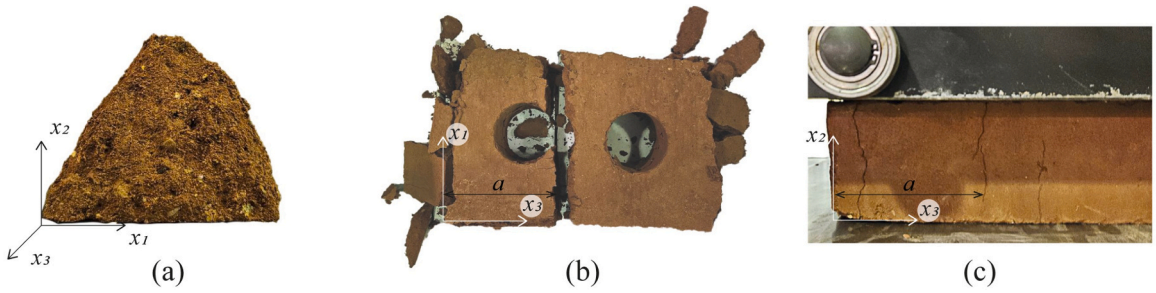


Fig. 5. Failure modes of saturated compressive testing. (a) X-shaped crack pattern in cubic specimens, (b) SCEB units after failure and (c) cracking development attributable to localized tensile stresses induced by surface non-planarity during loading.

also reported for stabilization systems combining cement with additional additives [33,73,74], within which the present results fall in the upper range of reported values. It should be noted that such comparisons are indicative, as material strength is also influenced by soil composition, manufacturing process, and testing conditions.

For full block specimens tested in dry conditions, the compressive strength obtained for the two block typologies was comparable, and an average value was adopted as representative for the SCEB unit as reported in subsection "Compression test on full block specimens".

Compressive strength measured on full block specimens was approximately 28% higher than that obtained on cubic specimens (see Table 2). The non-cubic geometry of full blocks may promote the development of transverse stress components and a less uniform stress distribution, leading to higher apparent strength values. In addition, the different surface-to-volume ratio of the two configurations may further influence boundary effects during testing, thereby affecting the measured compressive strength. These results indicate a marked sensitivity of the measured mechanical response to specimen geometry in earthen materials.

Regarding water absorption, cubic specimens consistently absorbed slightly more water than full block specimens (see Table 1). Although the relative difference, defined as $\left(A_w^b - A_w^{FB}\right)/A_w^{FB}\cdot 100$, is limited to approximately 8%, this observation is consistent with a marginally higher water uptake capacity in the inner portion of the material, possibly associated with density gradients induced by surface compaction during block manufacturing. Overall absorption values remain within the typical range reported for stabilized compressed earth blocks (approximately 5%–20%), as documented in previous studies [60,66,75].

The saturated results were interpreted with reference to the CRAterre guidelines [68,76], which indicate that stabilized earth blocks should not exhibit a reduction in compressive strength exceeding 50% under saturated conditions. Cubic specimens with a strength retention of approximately 48% satisfy this threshold. Full block specimens, with a mean retention of approximately 38%, fall below this limit, although one specimen exhibited a retention of 65%.

The differences in saturated behavior between the two geometric configurations can be partially attributed to geometric factors.

Full blocks often exhibit limited planarity of the loading faces ($x_1 - x_3$ plane), which may result in non-uniform contact with the loading plates. Under these conditions the applied load may not be uniformly distributed, leading to the development of local bending effects and associated transverse tensile stresses. These mechanisms are likely amplified under saturated conditions, where the reduced stiffness and cohesion of the material lower the resistance leading to premature cracking and failure. Cracking was frequently observed in correspondence with the void regions, where the effective cross-section is reduced and tensile stresses can more easily induce failure (see Fig. 5b). For these reasons, when full blocks are tested instead of extracted specimens, geometric irregularities may affect the stress distribution and influence the measured compressive strength. The relatively high variability observed for compressive strength in saturated full block specimens (COV = 0.37) may be associated with the testing and specimen-related limitations discussed above.

It should be noted that the strength retention of approximately 38% recorded for full block specimens is likely not representative of the effective saturated compressive strength of the material, as the measured response is influenced by geometric irregularities and boundary condition effects specific to this configuration, as discussed above. Cubic specimens, which better approximate uniaxial compression and are less affected by geometric irregularities, exhibited a retention of approximately 48%, satisfying CRAterre guidelines. On this basis, the material can be considered to meet the minimum durability requirements for stabilized earth blocks under moisture exposure.

3.2.2. Flexural tests

The flexural behavior of SCEB units was investigated by means of three-point and four-point bending tests performed on prismatic specimens cut from the blocks. In the three-point configuration, a total of three specimens were tested over a support span of 230 mm. The tests were conducted under displacement control, with a central point load applied at a rate of 0.5 mm/min. In the four-point configuration, three specimens were tested with a loading span equal to 1/3 of the support span, selected to reduce shear effects and favor a bending-dominated response. Two strain gauges were installed at midspan on the $x_1 - x_3$ plane, aligned with x_1 direction (see Fig. 6), to record compressive and tensile strains at the outer fibers. The gauges (Micro-Epsilon PL-60–11, 120 Ω, gauge length 60 mm), were adhesively bonded to the specimen surface using cyanoacrylate adhesive.

Flexural strength in the three-point configuration was determined as $f_{3f}^b = 3F_2L/\left(2bh^2\right)$, in accordance with UNI EN 1015–11 [77], where F_2 is the load at failure, L the support span length, and b and h the specimen width and height, respectively. Flexural strength in the four-point configuration was calculated following ASTM D6272 [78] for four-point bending test with loading span equal to 1/3 of the support span as $f_{4f}^b = F_2L/\left(bh^2\right)$. The flexural modulus E_f^b was determined as the tangent slope of the linear portion of the stress-strain response taking

Table 2
Compressive strength parameters of SCEB specimens: superscript *b* denotes specimens extracted from the block; *FB* denotes full block specimens.

	$\langle f_c^b \rangle$			$\langle f_c^{FB} \rangle$			$\langle f_c^{b,s} \rangle$			$\langle f_c^{FB,s} \rangle$		
	n	[MPa]	COV	n	[MPa]	COV	n	[MPa]	COV	n	[MPa]	COV
SCEB	13	5.9	0.11	6	8.4	0.17	5	2.8	0.14	6	3.3	0.35

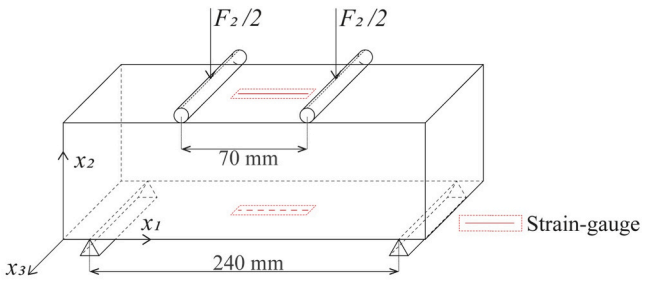


Fig. 6. Experimental setup for four-point bending test on SCEB prismatic specimens.

into account the deformation ε_{1t} recorded at the outer tensile fibers.

The specimens exhibited a brittle failure mode, characterized by limited deformation capacity. The mean flexural strength was $\langle f^b_{3f}\rangle = 1.14$ MPa (COV = 0.06) and $\langle f^b_{4f}\rangle = 1.17$ MPa (COV = 0.12) under three-point and four-point bending configurations, respectively. The indirect tensile strength, estimated from the four-point flexural strength following the relation $f^b_{ct} = 0.6 f^b_{4f}$ [79], is $f^b_{ct} = 0.71$ MPa. Following [79], tensile strength can be deduced from compressive strength as $f^b_{ctm} = 0.3\sqrt[3]{\left(f^b_c\right)^2}$. Following the latter formulation, tensile strength is $f^b_{ctm} = 0.98$ MPa.

The maximum strains recorded at outer tensile and compressed fibers were of $\langle \varepsilon^b_{1t}\rangle = 2.13 \times 10^{-4}$ and $\langle \varepsilon^b_{1c}\rangle = 1.58 \times 10^{-4}$. From these measurements, the neutral axis was located at 38.4 mm from the outer compressed fiber and 51.6 mm from the outer tensile fiber. For a square cross-section of side 90 mm, the centroidal axis is located at 45 mm, the neutral axis therefore deviates by 6.6 mm from the centroidal axis (7% of the section height). The corresponding flexural modulus was calculated as $E^b_f = 5600$ MPa (COV = 0.12).

The flexural strength values obtained are consistent with the upper range of those reported in CRAterre guidelines for SCEB [68]. The estimated tensile strength is significantly lower than the compressive strength, indicating a quasi-brittle behavior with very limited tensile capacity (see Table 3). An alternative estimation of tensile strength based on compressive strength, following [64], yields $f^b_{ctm} = 0.98$ MPa, compared to $f^b_{ct} = 0.71$ MPa obtained from flexural tests. This difference indicates that the evaluated tensile strength is sensitive to the adopted formulation; however, the relative discrepancy (27%) does not significantly affect the interpretation of the material as having a low tensile capacity.

The position of the neutral axis and the overall mechanical response suggest that, at this stage of the research, the material can be reasonably approximated as isotropic. The percentage difference, roughly 19%, between the elastic modulus derived from flexural tests and that obtained from compression (see Table 4) is not sufficiently large to indicate a fundamentally different mechanical behavior, and can be attributed to material heterogeneity, test setup, and specimen geometry.

In this context, the material may be reasonably modeled as an isotropic elasto-fragile material with negligible tensile strength.

Table 3
Flexural strength parameters of SCEB specimens. COV values of f^b_{4f} and f^b_{ct} are the same because tensile strength is indirectly derived from flexural strength.

	$\langle f^b_{3f}\rangle$			$\langle f^b_{4f}\rangle$			$\langle f^b_{ct}\rangle$		
	n	[MPa]	COV	n	[MPa]	COV	n	[MPa]	COV
SCEB	3	1.14	0.06	3	1.17	0.12	3	0.71	0.12

3.3. Mechanical characterization of earth-based mortars

Masonry mechanical response is governed by the combined behavior of units and mortar, with the latter affecting force transfer and deformation compatibility within the system. Modifying mortar composition is therefore a common strategy to enhance deformation capacity, while potentially reducing strength and stiffness. The objective is to improve deformation capacity while preserving adequate mechanical strength, using materials compatible with low-impact and locally sourced construction; hence, the mechanical response of an earth-based mortar and of the same mix reinforced with dispersed natural fibers is investigated.

Three mortar mixes were produced. All mixes consisted of sieved red earth, sand, and cement in a mass ratio of 3:6:1.

Mortar production is artisanal, with the water content defined in-situ to achieve optimal workability, roughly 40% of the dry mass. When the fibers were included in the mixture, water content was increased to reach the same optimum level of mortar workability. The increase in water content was based on practical considerations, the consistency of non-reinforced mortar mix was taken as reference.

Mix-1 was an unreinforced earth mortar, with a density of $\rho^{m,m1} = 1600$ kg/m^3 (COV = 0.029). Mix-2 incorporated hemp fibers at 1.8% by dry mass, a fiber content within the range reported in the literature [80], density of $\rho^{m,m2} = 1566$kg/m^3 (COV = 0.012). Mix-3 incorporated coconut fibers at the same fiber content, with a density of $\rho^{m,m3} = 1558$ kg/m^3 (COV = 0.026). Fibers with a nominal length of approximately 20 mm were incorporated into the dry constituents prior to the addition of water.

The fibers were incorporated without pre-treatment and no specific mechanical characterization was performed, as the objective of this study was not to evaluate the intrinsic properties of the fibers, but rather to investigate the feasibility of their inclusion in earth-based mortar, using locally available materials. Fiber treatment procedures would introduce additional processing steps that are not typically compatible with semi-artisanal construction practices.

Although natural fibers are known to exhibit limited durability in alkaline environments, primarily due to alkaline attack and calcium hydroxide-induced mineralization that lead to embrittlement and progressive loss of mechanical properties in cementitious matrices [81,82], this remains an active area of research, particularly regarding durability enhancement through fiber treatments and coatings [83].

The cement content of the earth-based mortar adopted in this study is lower than that of conventional cement-based composites. For this reason, untreated fibers were considered to carry out a preliminary evaluation of their potential benefits within the specific mortar formulation investigated. Mortar specimens were then prepared according to UNI EN 1015–11 and cured for 28 days under laboratory conditions (18 °C, 45% relative humidity) to allow adequate development of cementitious strength. Shrinkage was calculated after the period as the percentage difference between the reference mold dimension and the measured specimen length along the same direction x_i, according to $\varepsilon^s_i = \left(l^{ref}_i - l^m_i\right)/l^{ref}_i$. The shrinkage levels $\langle \varepsilon^s_i\rangle$, measured along the three principal directions, are reported below for the three mortar mixes:

- Mix-1: $\langle \varepsilon^s_1\rangle = 0.40\%$, $\langle \varepsilon^s_2\rangle = 2.50\%$, $\langle \varepsilon^s_3\rangle = 1.09\%$;
- Mix-2: $\langle \varepsilon^s_1\rangle = 0.19\%$, $\langle \varepsilon^s_2\rangle = 2.08\%$, $\langle \varepsilon^s_3\rangle = 1.04\%$;
- Mix-3: $\langle \varepsilon^s_1\rangle = 0.11\%$, $\langle \varepsilon^s_2\rangle = 0.64\%$, $\langle \varepsilon^s_3\rangle = 0.40\%$.

Compared to the unreinforced mortar, fiber-reinforced mixes exhibited a systematic reduction in shrinkage along all directions, consistent with previous studies [84–87]. Nevertheless, shrinkage levels remained markedly higher than those typically reported for conventional cementitious mortars, a behavior commonly associated with the presence of clay-rich constituents [86,88].

Table 4
Elastic parameters of SCEB specimens.

	$\langle E^b \rangle$			$\langle \nu^b \rangle$			$\langle E_f^b \rangle$		
	n	[MPa]	COV	n	[MPa]	COV	n	[MPa]	COV
SCEB	13	6898	0.4	13	0.34	0.37	3	5600	0.12

3.3.1. *Flexural tests*

The three-point bending test setup was defined in accordance with standard recommendations. Tests were carried out under displacement control at a rate of 0.5 mm/min. Six specimens for Mix-1 and Mix-2 mortars were tested, and four Mix-3 specimens. Prior to testing, most of the Mix-3 specimens exhibited visible cracking or partial splitting, indicating reduced structural integrity already at the specimen preparation stage (see Fig. 7). This behavior may be related to the presence of coconut fibers, which can interfere with curing in earth-based mortars. Coconut fibers are characterized by a high water absorption capacity, which can adversely influence the mechanical response of moisture-sensitive matrices [89]. Previous studies on fiber-reinforced cementitious materials have shown that the incorporation of natural fibers may promote swelling phenomena and interfacial debonding, resulting in a reduction in tensile and flexural strength [89,90]. In earth-based matrices, the pronounced hygroscopic behavior of coconut fibers may increase the internal moisture content, triggering similar mechanisms. In this context, the poor flexural performance observed for Mix-3 mortar, together with the presence of pre-existing cracking, is consistent with a fiber-induced increase in moisture and associated disruption of matrix continuity. These effects can reasonably be linked to the loss of mechanical integrity recorded for the coconut fiber–reinforced mortar. Within the investigated configuration, their inclusion did not result in a beneficial effect on the flexural response of the cement-stabilized earth mortar. Accordingly, coconut fiber reinforcement was not further investigated within the scope of the present experimental program.

All mortar mixes exhibited limited flexural strength, consistent with values typically reported for earthen mortars and clay-based materials in the literature [84,91,92]. Among them, Mix-1 showed the highest flexural performance. Mix-2 specimens exhibited lower strength than Mix-1 but remained within a comparable range (see Table 5). Although no strength enhancement, typically associated with hemp fiber reinforcement, was observed, Mix-2 specimens displayed a clear increase in deformation capacity, with a 160% increase in vertical displacement u_2 relative to Mix-1 (see Fig. 8). The absence of strength gain may be related to the selected fiber content.

3.3.2. *Compression tests on mortars*

To evaluate the compressive strength and elastic modulus of Mix-1 and Mix-2, uniaxial compression tests were performed. While standard procedures prescribe testing mortar halves using a dedicated loading frame, this configuration does not readily allow for strain measurement required for elastic modulus determination. A modified setup was then adopted. Cubic specimens with nominal dimensions of $40 \times 40 \times 40\text{mm}^3$ were extracted from the mortar halves, enabling direct strain measurement while preserving the loading conditions prescribed by the standard (see Fig. 9). The resulting loaded area was defined to be equivalent to the standard configuration, ensuring consistency in stress evaluation. A total of six specimens were tested for both the unreinforced mortar and for the hemp fiber reinforced mortar.

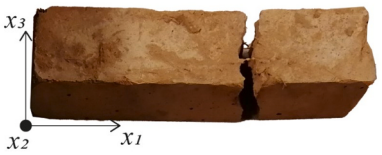


Fig. 7. Earth-based mortars, Mix-3 specimens damaged prior to testing.

The same compression test setup adopted for the block specimens was also used for the mortar cubes (see Section 3.2.1, "Compression test on cubic specimens"). No surface regularization of the contact faces was performed. Although no evident irregularities were detected through visual inspection, this aspect is acknowledged as a possible limitation of the experimental investigation, since local irregularities at the contact surfaces may influence the stress distribution and, consequently, the mechanical response in both the linear and nonlinear stages. Due to the sandy surface texture and friability of the specimens, conventional contact extensometers could not be reliably employed. For this reason, Digital Image Correlation (DIC) was adopted as a virtual extensometer [93,94]. The homogeneous color and granular surface of the mortar limited the identification of stable tracking points on the specimen itself; therefore, a textured reference element was positioned on the same plane as the specimen (reference point 1), with the actuator load transfer plate used to track a second reference point (see Fig. 10). While the setup allowed for ε_2 extraction, accurate measurement of ε_1 was not achievable, preventing the experimental definition of the Poisson ratio as defined in subsection "Compression test on cubic specimens". The value was therefore assigned based on the mortar strength class.

Compressive loading was applied under displacement control at a constant rate of 0.5 mm/min. As neither the failure mode nor the time to failure could be anticipated, continuous video acquisition was performed throughout each test. Video recordings were acquired using a Nikon D5600 DSLR camera at 50 fps, corresponding to a sampling frequency of 50 Hz. Frames were subsequently extracted in post-processing at a frequency of 1 Hz, following visual inspection of the footage, as this interval provided sufficient temporal resolution for both failure observation and DIC analysis while limiting the associated computational demand.

The compressive strengths of Mix-1 and Mix-2 mortars were comparable, although a slight reduction was observed for Mix-2, consistent with previous studies reporting that fiber incorporation in earthen mortars can result in a reduction in strength [87,95,96]. Mix-1 specimens failed through sudden vertical splitting accompanied by corner crumbling (see Fig. 11), indicative of a brittle response and qualitatively consistent with failure modes reported for concrete cubes in UNI EN 12390–3, as well as for earth-based mortars without fiber reinforcement [85]. In contrast, Mix-2 specimens exhibited delayed failure characterized by the development of multiple vertical cracks. The presence of hemp fibers appears to contribute to enhanced crack bridging and delayed crack propagation, leading to increased deformation capacity without a corresponding increase in compressive strength (see Fig. 11). As a result, the failure mode becomes more diffuse and cannot be readily classified within conventional brittle failure typologies.

The elastic modulus E^m was evaluated from the initial slope of the stress–strain curve (see Fig. 12). Mix-1 exhibited a higher stiffness than Mix-2, while reaching lower maximum strain levels. The maximum vertical strains were $\langle \varepsilon_2^{m,m1} \rangle = 0.011$, $\langle \varepsilon_2^{m,m2} \rangle = 0.19$. Accordingly, Mix-1 was selected as the reference mortar for the masonry tests, as it provides an appropriate balance between stiffness and strength while maintaining a deformation capacity higher than that of the blocks (see Fig. 13), thereby ensuring strain compatibility within the masonry.

4. Mechanical characterization of masonry meso-scale

Following the characterization of the constituent materials, the experimental campaign was extended to the meso-scale to investigate

Table 5
Mechanical parameters of earth-based mortars.

	$\langle f_f^m \rangle$			$\langle u_2^m \rangle$			$\langle f_c^m \rangle$			$\langle E^m \rangle$	
	n	[MPa]	COV	n	[mm]	COV	n	[MPa]	COV	n	[MPa]	COV
Mix-1	6	0.59	0.06	6	0.6	0.11	6	1.3	0.18	6	214	0.22
Mix-2	6	0.36	0.14	6	1.57	0.02	6	0.9	0.21	6	20	0.29
Mix-3	4	0.04	0.22	-	-	-	-	-	-	-	-	-

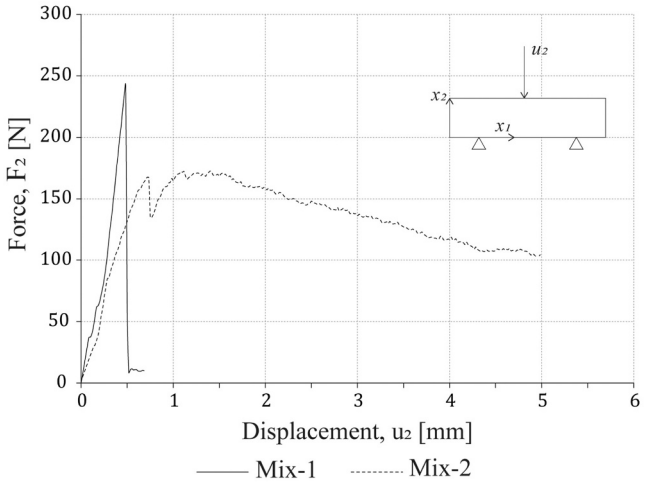


Fig. 8. Force-displacement plot of representative Mix-1 and Mix-2 mortars specimens tested in three-point bending along x_2 direction.

the mechanical response of masonry. The tested configuration consisted of a header-bond masonry panel with uniform mortar joints of thickness $e = 5$ mm and overall dimensions of $1225 \times 945 \times 305 \text{mm}^3$, as shown in Fig. 14.

As the presented research is part of a larger study, testing on unreinforced panels was a preliminary step to characterize unreinforced masonry behavior. The panel dimensions were defined to allow casting of the reinforcement frame while keeping specimen dimensions contained, and without significantly altering the frame-to-masonry ratio.

The test setup was defined in accordance with UNI EN 1052–1 [97]. To promote uniform stress transfer, a thin layer of weak cementitious mortar was applied to the top and bottom surfaces of the panel. In the absence of a specific design code for cement-stabilized CEB masonry, conventional masonry standards were applied by analogy, as commonly adopted in the literature for stabilized earth masonry construction [19].

The masonry panels were cured for 28 days prior to testing under laboratory conditions (18 °C, 45% relative humidity). This curing period ensured the proper development of the cementitious matrix within the mortar joints.

Uniaxial compression tests were performed under displacement control at a constant rate of 1.5 mm/min, corresponding to a strain rate of approximately 2.6×10^{-5} s^{-1} for the 945 mm high specimen. Hence, the adopted loading rate falls within the quasi-static regime commonly reported in the literature. Owing to the inherent material and structural



Fig. 11. Failure typologies of mortar cubic specimens tested in compression: Mix-1 specimens (back row) and Mix-2 specimens (front row).

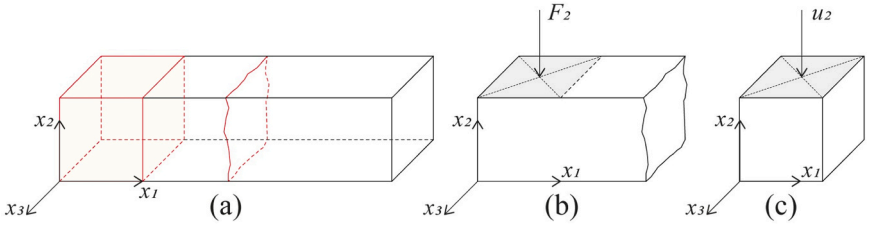


Fig. 9. Mortar specimens: (a) mortar halves from three-point bending test; definition of specimen for compression test (b) in accordance with the standard and (c) with modified configuration.

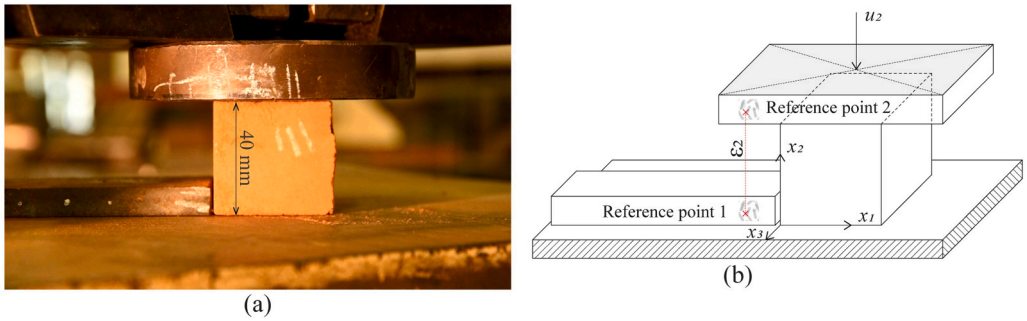


Fig. 10. Experimental setup of compression test on mortar cubes: (a) test configuration with indication of mortar cube dimension; (b) schematic representation of the DIC setup with ε_2 extraction points reference.

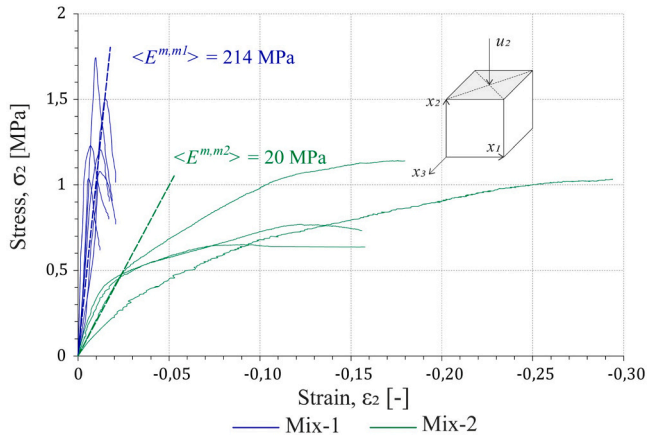


Fig. 12. Stress-strain plot of Mix-1 and Mix-2 mortar cubic specimen tested in compression, x_2 direction.

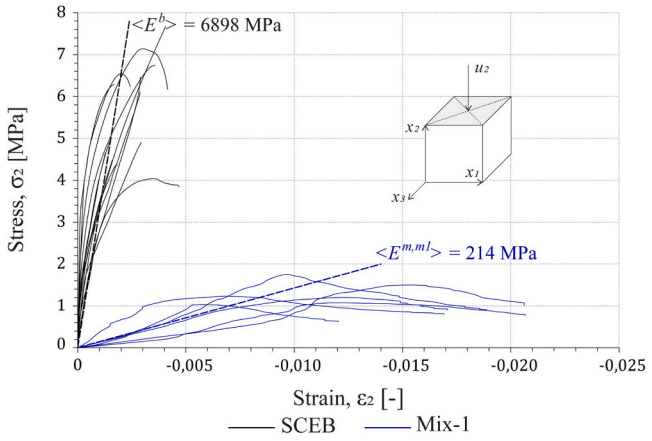


Fig. 13. Stress-strain plot of SCEB cubes and Mix-1 mortar cubes tested in compression along x_2 direction.

heterogeneity of earthen masonry, crack initiation and failure patterns could not be predicted a priori. Accordingly, DIC was employed to monitor in-plane deformations in the x_1–x_2 plane (see Fig. 14c). High-contrast markers were applied to the panel surface, with two markers placed on each block head to track unit-level damage (Fig. 14b), producing a regular marker grid across the specimen. When required, the natural texture of the earthen surface was used to supplement point tracking. Additional reference markers were placed on the concrete support beam to provide a stable, non-deformable reference. Images were acquired at interval $\Delta t = 2$ s.

The global vertical strain ε_2^{EM}, was evaluated using DIC markers placed on the second and ninth masonry courses, defining a representative gauge length. Adopting the central third as reference was not considered appropriate, as the specimen height-to-unit ratio would include only a limited number of masonry courses, leading to a non-representative strain evaluation at the assemblage scale. Furthermore, the first and last courses were excluded to minimize boundary effects associated with local crushing at the loading interfaces, which would otherwise result in an overestimation of the panel deformation. Accordingly, the region between the second and ninth courses was adopted as a representative measure of the masonry response. The global axial strain for each specimen was obtained by averaging the vertical deformation measured between the selected courses along the length of the panel.

To evaluate the elastic response of the earthen masonry under compression, the limit of the elastic regime was defined as the onset of cracking within the panel. Since crack initiation cannot be reliably identified from the global stress–strain response alone, a local strain-based criterion was adopted. Local deformation along the x_1 direction, ε_1, was monitored across all masonry units within the panel. Given the heterogeneous and artisanal nature of the constituent materials, the location of crack initiation could not be determined a priori. The transition from linear to non-linear response was identified by a clear increase in local transversal strain within the block where strain localization was first detected (see Fig. 15). It is worth noting that this criterion does not aim to characterize the response of an individual block in isolation, but rather to identify the onset of damage within the masonry assembly as a whole, which constitutes the relevant scale for the definition of the elastic limit state. The corresponding time instant was then mapped onto the global stress–strain response in the x_2 direction. The stress–strain state corresponding to this instant was taken as the limit of the elastic regime, and the elastic modulus of the masonry in the loading direction, denoted as $E_2^{EM,el}$, was evaluated from the initial slope of the global stress–strain curve up to this limit.

Two wallettes, denoted EM1 and EM2, were tested. Both specimens exhibited a limited linear elastic response in the initial portion of the curve, followed by a peak stress of approximately $\langle f_c^{EM} \rangle = 1.94$MPa. A

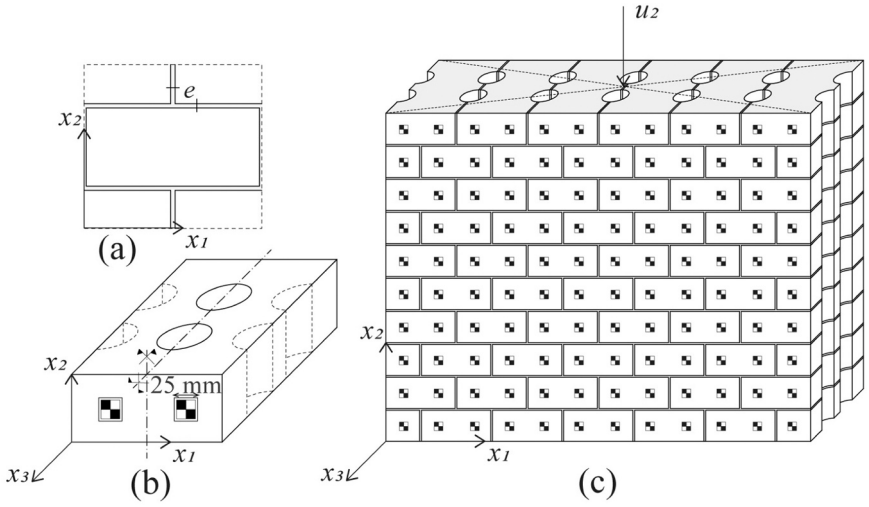


Fig. 14. Masonry wallettes for compression tests. (a) Mortar joint thicknesses $e = 5$ mm, (b) local marker placement on full block to monitor unit-level deformation, and (c) panel layout with high-contrast markers distributed across the x_1 –x_2 plane.

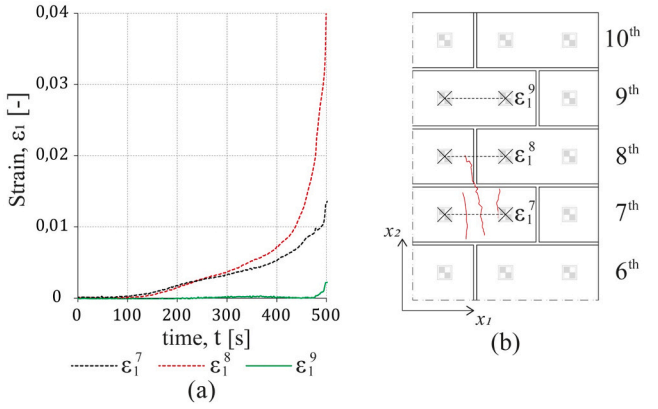


Fig. 15. Crack initiation at the unit–head joint/unit interface. (a) Strain–time response in the x_1 direction for two monitoring points; (b) localization of initial cracking along the $x_1 - x_2$ plane. Rows are numbered from 1 (bottom) to 10 (top).

sudden drop in load-carrying capacity was observed immediately after the peak, indicating a brittle failure behavior (see Fig. 16).

In both cases, initial cracking was observed at the unit level. Unlike conventional brick masonry, where cracks typically initiate near mid-span, cracking developed at locations corresponding to reduced cross-sections within the blocks, approximately at one-third or one-sixth of the block head length depending on the block geometry (see Fig. 17). Cracks propagated vertically through the underlying units without a consistent preference for a specific block type. In both specimens, final failure was characterized by the formation of continuous vertical cracks extending along the height of the wallettes (see Fig. 18).

For comparison purposes, the elastic modulus was also evaluated following the UNI standard definition ($E_2^{EM,st}$), i.e., as the secant modulus corresponding to one-third of the maximum compressive stress. The values obtained using the two definitions show noticeable differences, both in magnitude and relative ranking between specimens. For specimen EM1, the elastic modulus $E_2^{EM1,el}$, determined using the proposed approach, exceeds the secant modulus $E_2^{EM1,st}$, whereas the opposite trend is observed for specimen EM2 (see Table 6).

The compressive strength of the SCEB masonry assemblages obtained in the present study (see Table 6) is consistent with values reported in the literature for cement-stabilized compressed earth block masonry, which ranges from approximately 1.2–3.3 MPa depending on the mortar type and specimen geometry [98–100]. The result exceeds values reported for adobe-based systems with comparable mortar strength [101, 102] confirming the beneficial role of cement stabilization in improving

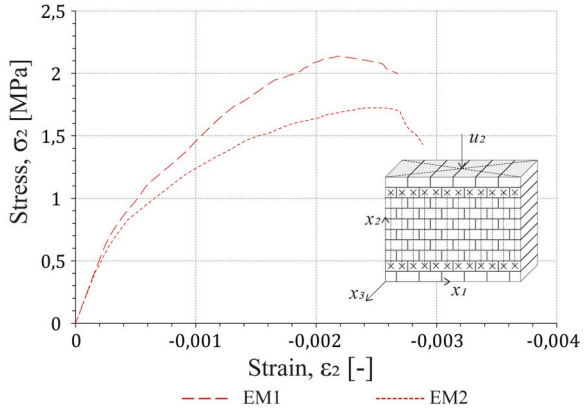


Fig. 16. Stress-strain plot of earth wallettes tested in compression along x_2 direction.

the mechanical performance of the masonry assemblage. The relatively lower strength compared to systems using cement-sand mortar is consistent with the influence of mortar compressive strength on masonry response reported in the literature [98,102].

The sensitivity of the elastic modulus to the definition adopted, i.e., to the method used for its evaluation, suggests that the choice of evaluation method significantly affects the measured value and may therefore influence comparative assessments across studies. This sensitivity may be partially linked to the inherent heterogeneity of earthen materials and the variability associated with artisanal production processes, which can produce a non-uniform stress-strain response.

5. Numerical analysis

To describe the heterogeneous mechanical behavior of cement-stabilized CEB masonry, a macro-modeling strategy was adopted. The effective elastic properties of the masonry were derived through a homogenization procedure based on the mechanical response at the unit–mortar scale [103–106]. In the following section, two Cartesian systems are used: x_1, x_2, x_3, at the macro-level, whereas y_1, y_2, y_3 at the micro-level, in accordance with the homogenization procedure. For single-leaf masonry structures, a two-dimensional representative volume element (REV) is commonly assumed, due to the geometric and material uniformity of the system along the third dimension. Three-dimensional homogenization can be required when the masonry response is influenced by out-of-plane effects, as discussed by Cecchi and Sab [107]. In the present study, however, the masonry assemblage is periodic along x_3 direction due to the presence of the voids, which characterize the two typologies of block adopted (see Fig. 1a). In this context, a three-dimensional homogenization approach was employed. The 3D REV is defined as shown in Fig. 19a, with the v_1 and v_2 representing directions of periodic replication with respect to the $x_1 - x_2$ plane.

Due to geometric symmetry, only one-eighth of the representative cell was modeled for the homogenization analysis (see Fig. 19b). The elastic properties of SCEBs and earth-based mortar, experimentally determined, were used to define the material properties of the cell constituents. The homogenization problem was solved using a displacement-based formulation implemented in the Straus7 finite element (FE) code. The resulting homogenized properties are reported in Table 7.

The homogenized elastic modulus in the loading direction ($E_2^H = 2398$ MPa), obtained using the experimentally determined properties of the constituent materials, was compared with values derived from wallette compression tests. The elastic modulus evaluated according to standard practice at one-third of the peak load ($E_2^{EM,st}$) was equal to 2172 MPa, corresponding to a deviation of −9% with respect to the homogenized value. When the elastic modulus was instead evaluated at the end of the experimentally identified elastic regime ($E_2^{EM,el} = 2390$ MPa), the deviation was reduced to −0.33%. This comparison indicates that the elastic modulus defined on the basis of the pre-cracking response is more consistent with the assumptions underlying the homogenization procedure, which is formulated within the framework of linear elasticity. While the one-third peak method provides a rapid and standardized estimate of stiffness, an elastic-limit-based definition enables a more rigorous comparison between experimental results and homogenized predictions in the context of model verification. In order to investigate the influence of internal voids on the elastic response in the x_1–x_2 plane, a two-dimensional representative volume element (2D REV) was additionally considered. The objective of this analysis was to assess whether the presence of voids affects the macroscopic elastic properties when the material constituents remain unchanged. The first 2D REV was defined by directly extracting the y_1–y_2 external plane of the three-dimensional cell (see Fig. 20b), while preserving the same geometry and material properties. A second two-

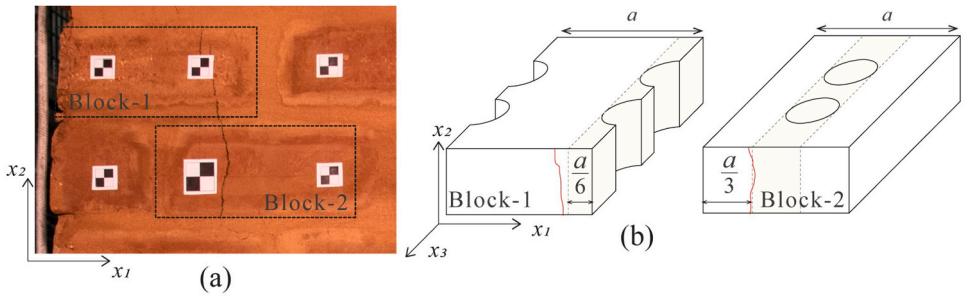


Fig. 17. Crack propagation in SCEB masonry, (a) localization on specimen surface ($x_1 - x_2$ plane) and (b) schematic representation of the observed crack with respect to blocks geometry.

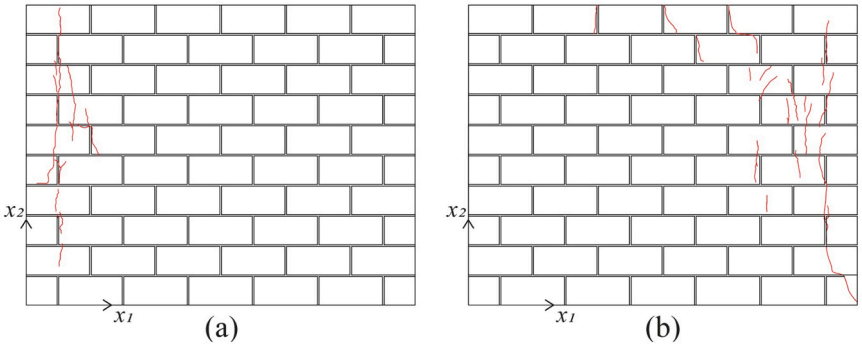


Fig. 18. Crack pattern of (a) EM1 and (b) EM2 specimen tested in compression, x_2 direction.

Table 6
Mechanical properties of cement-stabilized CEB masonry panels.

Specimen	f_c^{EM} [MPa]	$E_2^{EM,el}$ [MPa]	$E_2^{EM,st}$ [MPa]
EM1	2.14	2540	1945
EM2	1.73	2240	2400
⟨EM⟩	1.94	2390	2172

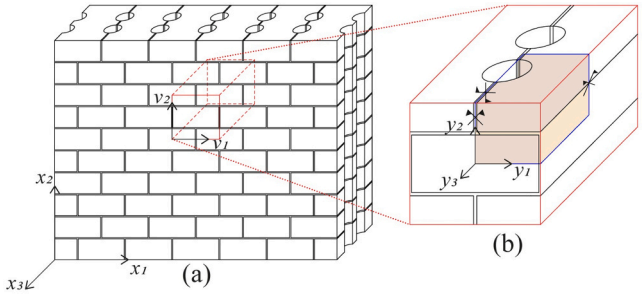


Fig. 19. Definition of the representative volume element (REV). (a) REV identification within the masonry panel, (b) geometric configuration of the 3D cell.

Table 7
Homogenized media elastic parameters.

$E_1^H = 3180$ MPa	$\nu_{12}^H = 0.204$	$\nu_{21}^H = 0.175$	$G_{12}^H = 742$ MPa
$E_2^H = 2398$ MPa	$\nu_{23}^H = 0.122$	$\nu_{32}^H = 0.245$	$G_{23}^H = 1150$ MPa
$E_3^H = 5479$ MPa	$\nu_{13}^H = 0.160$	$\nu_{31}^H = 0.275$	$G_{13}^H = 1160$ MPa

dimensional configuration (denoted as $2D^R$) was then introduced, in which the dimension along the y_1 direction was reduced to account for the minimum effective cross-section associated with the void geometry of the three-dimensional cell along the y_3 direction (see Fig. 20c). The reduction was applied exclusively to the block dimension, while the mortar joints were kept unaltered, so that the overall masonry texture remained unchanged and only the effective block cross-section was modified. In both configurations, the mechanical properties of the constituent materials were kept identical to those used in the three-dimensional homogenization. The objective of this simplification was to evaluate whether a reduced two-dimensional cell, obtained by modifying only the block dimension, could reproduce the in-plane elastic response of the corresponding three-dimensional configuration with internal voids, thereby offering a computationally efficient alternative to full three-dimensional homogenization. The two-dimensional investigation provides a controlled framework in which material properties are kept constant, allowing differences in the in-plane elastic response to be attributed exclusively to geometric effects associated with the presence or omission of voids.

As a result, the two-dimensional homogenization framework leads to a closer agreement only along the direction aligned with the void axis, as reflected by the smaller overestimation of $E_2^{H,2D}$ (+17.9%), where cross-sectional continuity is preserved. In contrast, the model significantly overestimates stiffness in the direction orthogonal to the voids, with increases in E_1 (+31.2%) and G_{12} (+18.2%), indicating that the material discontinuities governing load transfer in the three-dimensional configuration are not adequately captured (see Table 8). The Poisson ratios exhibit substantial deviation from the three-dimensional reference, particularly overestimating ν_{21}, highlighting a marked amplification of transverse deformation coupling. Overall, these results indicate that a purely two-dimensional homogenization remains insufficient for representing the anisotropic elastic response of the masonry assemblage, even when the voids are aligned with the principal loading direction. The second $2D^R$ REV, refined to account for the minimum effective cross-sectional area of the blocks, shows an improved agreement with the three-dimensional homogenization results for $E_1^{H,2D^R}$, with deviation reduced to 7%, while E_2 and G_{12} still overestimating the stiffness, with no substantial benefit compared to 2D configuration. The Poisson ratios

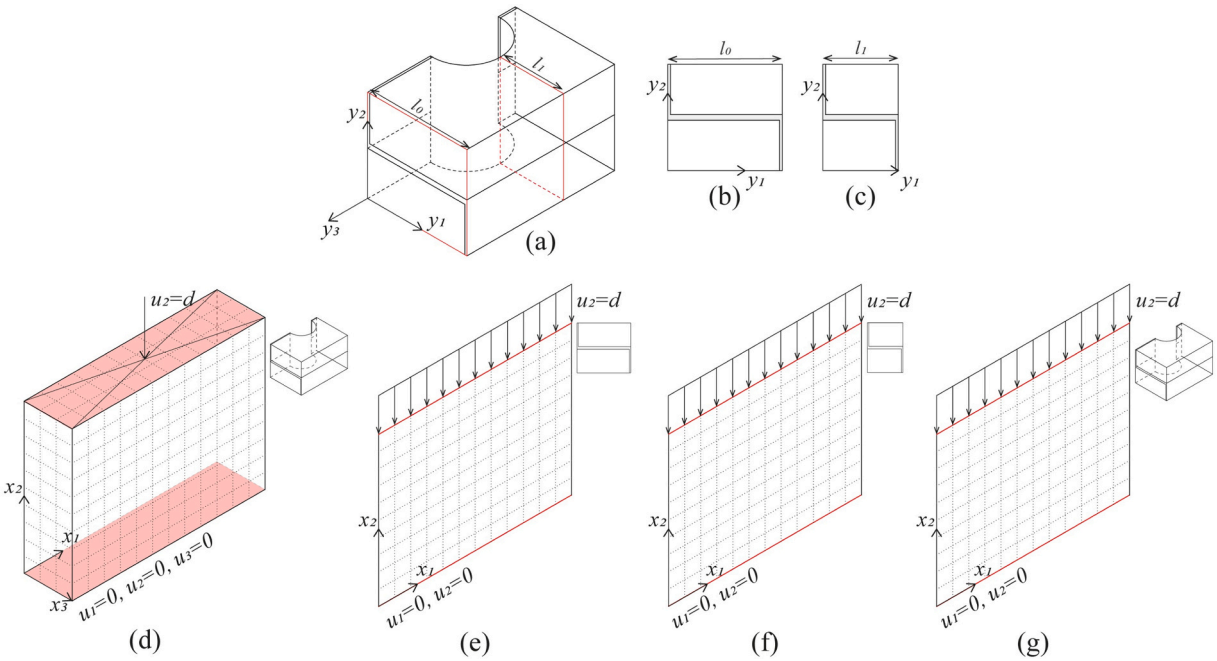


Fig. 20. REV configurations and corresponding numerical models: (a) 3D unit cell with cylindrical void; (b) 2D cell based on masonry pattern; (c) reduced 2D cell ($2D^R$) accounting for the maximum cross-section reduction along the y_1 axis; (d) model A; (e) model B; (f) model C; (g) model D.

Table 8
Comparison of homogenized media mechanical parameters between two-dimensional and three-dimensional analysis.

Cell	E_1^H [MPa]	E_2^H [MPa]	ν_{12}^H [-]	ν_{21}^H [-]	G_{12}^H [MPa]
3D	3180	2398	0.204	0.175	742
2D	4172	2826	0.219	0.323	877
$2D^R$	3394	2797	0.224	0.272	886

remain significantly higher than in the three-dimensional case, particularly ν_{21}. Overall, the $2D^R$ configuration improves the prediction of stiffness components associated with directions perpendicular to the void axes but remains inadequate for reproducing the full anisotropic elastic response, which requires a three-dimensional description (see Table 8).

A linear elastic analysis was performed on four orthotropic macro-models to systematically isolate the independent contributions of two modeling choices: the dimensional assumption at the macro-scale (3D vs. 2D plane stress) and the homogenization scheme adopted at the micro-scale. The four configurations are defined as follows:

- Model A: elastic properties from 3D homogenization, and 3D macro-model, (Fig. 20a, Fig. 20d).
- Model B: elastic properties from 2D homogenization of a full-block REV, and 2D plane stress macro-model (Fig. 20b, Fig. 20e).
- Model C: elastic properties from 2D homogenization of a reduced block REV, with the 2D block length corresponding to the minimum 3D block cross-section at the void location, and 2D plane stress macro-model (Fig. 20c, Fig. 20f).
- Model D: elastic properties from 3D homogenization, and 2D plane stress macro-model to isolate the effect of the macro-model dimensional reduction from any simplification introduced at the micro-scale (Fig. 20a, Fig. 20g).

Uniaxial compression was imposed in accordance with the experimental configuration through a vertical displacement u_2 at the top surface and a fixed base. A single elastic modulus value E_2 is reported per model, as the analyses are conducted within the linear elastic domain under uniaxial compression, for which the response is fully described by a scalar stiffness measure. Results are summarized in Table 9.

As is well known, in the context of 2D macro-modeling, plane stress and plane strain formulations represent the upper and lower bounds of the 3D response, respectively. Accordingly, the plane stress models are expected to overestimate the stiffness with respect to the 3D reference, as confirmed by the results. Among the plane stress models, Model C reduces the overestimation of the elastic modulus E_2 to approximately 43% compared to over 75% for Model B, demonstrating the influence of the REV geometry in the homogenization procedure. Model D, which retains 3D homogenized properties within a 2D macro-model, shows the closest agreement among the 2D configurations with approximately 33% overestimation, confirming that the micro-scale homogenization scheme plays a more significant role than the macro-model dimensional assumption alone. The three-dimensional Model A shows the closest overall agreement with the experimental elastic response, confirming that 2D plane stress formulations remain inadequate for accurately reproducing the elastic behavior of masonry assemblages with internal voids.

To examine the non-linear compressive response of the masonry panels, a three-dimensional isotropic continuum model was developed using ANSYS. The non-linear model is intentionally preliminary, consistent with the scope of the present study. In the absence of a complete experimental characterization of non-linear material parameters and given the variability reported in the literature for stabilized earthen materials, a multi-linear stress–strain relationship was adopted, with the constitutive points directly derived from the experimentally measured mean stress–strain response of the masonry panels reported in Section 4 (see Fig. 18). The numerical model was not intended to reproduce post-peak behavior, which is not included in the constitutive

Table 9
Comparison of the elastic linear response of homogenized macro models tested in compression.

	Experimental	Model A	Model B	Model C	Model D
E_2 [MPa]	2390	2426	4211	3425	3173

definition. This limitation is consistent with the brittle failure observed experimentally and does not affect the interpretation of the pre-peak response. The simulated compressive response under axial loading in the x_2 direction captures the pre-peak experimental trend, supporting the use of the proposed modeling strategy for interpreting the response up to peak load (see Fig. 21).

6. Conclusions

This study presents an integrated experimental–numerical investigation of cement-stabilized compressed earth block (CEB) masonry, aimed at characterizing its mechanical response across material and unit scales within a consistent framework.

Block scale testing confirmed that specimen geometry and moisture significantly influence compressive strength: in full-scale SCEB units, geometric irregularities induce localized stress concentrations and premature failure in the saturated state. Fiber reinforcement increased mortar deformability but was associated with a reduction in stiffness and compressive strength within the investigated range of fiber content and fiber length. This behavior indicates that, within this range, fiber inclusion does not provide a mechanical advantage for structural mortar applications. On this basis, mortar selection was driven by mechanical compatibility with the masonry units rather than by the maximization of ductility, leading to the adoption of the unreinforced earth-based mortar as the reference material. Moreover, although no mechanical advantage was observed within the investigated range, this does not preclude the potential of fiber reinforcement. Once an appropriate dosage is defined, durability, degradation, and compatible fiber treatments should be further investigated in line with the artisanal construction approach. At the masonry scale, failure was governed by unit-level cracking initiated at geometric discontinuities within the blocks, leading to vertical crack propagation through the panel. The definition adopted for the elastic modulus was found to significantly influence the estimated stiffness of earthen masonry. Moduli derived from standard one-third peak stress definitions and those based on pre-cracking strain limits showed no clear correspondence. A strain-based definition of the elastic modulus, linked to the onset of local cracking, was found to be more consistent with the assumptions underlying the homogenization framework adopted in the numerical analysis. Three-dimensional homogenization was required to capture geometric features of the block morphology that are not described by the masonry texture and are intrinsically lost in two-dimensional representations. The nonlinear finite element model was formulated to reproduce the pre-peak compressive response of the masonry panels using homogenized elastic properties and an experimentally derived multi-linear stress–strain law. The analyses were confined to the pre-peak regime, in accordance with the brittle experimental response. The numerical models presented in this study are intentionally preliminary in scope, developed to support the characterization of the constituent materials and masonry assemblies as a foundation for the broader research program on reinforced earthen masonry assemblages.

Within this context, the results presented are subject to limitations related to the inherent variability of earthen materials, the limited number of tested specimens, and the semi-artisanal production process, which may affect the reproducibility of the mechanical response.

Overall, the combined experimental–numerical framework offers a coherent basis for interpreting the mechanical behavior of cement-stabilized compressed earth block masonry, particularly in contexts where material heterogeneity and limited experimental data constrain the applicability of conventional modelling approaches.

CRediT authorship contribution statement

Jacopo Baldelli: Writing – review & editing, Writing – original draft, Methodology, Investigation. **Giosuè Boscato:** Writing – original draft, Supervision, Methodology, Data curation. **Makhaly Ba:** Resources. **Antonella Cecchi:** Writing – review & editing, Supervision.

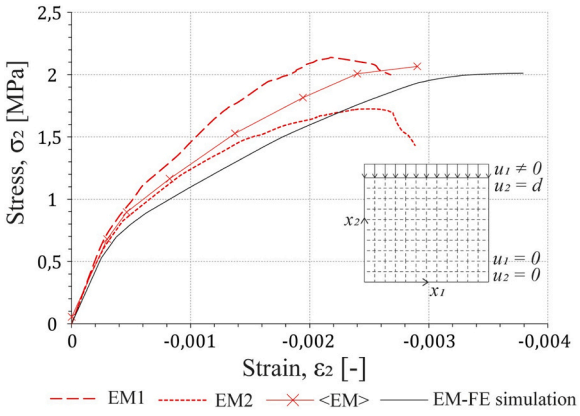


Fig. 21. Compressive response of the masonry panel: experimental curves, numerical simulation, and multilinear constitutive law defined from mean experimental stress–strain points (ε_2, σ_2).

Declaration of Competing Interest

The authors declare that they have no known competing financial interests or personal relationships that could have appeared to influence the work reported in this paper

Acknowledgments

The authors would like to thank Abdoulaye Petit Faye and Arch. Andrea Degan for providing the materials and facilitating access to the construction system investigated in this study. The authors also acknowledge the IUAV University Laboratory of Strength of Materials (LabSCo) for its valuable support during the experimental program. In addition, the authors acknowledge the Project “New Insights in the Mechanical Modeling of Cultural Heritage for Sustainable Restoration: Green Composites and Nano-Technologies” (GreNaTe, CUP: F53D23002060006). This work did not receive any direct financial support from the project. Finally, the authors thank Dr. Serigne Diop (PhD candidate) for his technical support.

Data availability

Data will be made available on request.

References

[1] Un-Habitat, World cities report 2020: The value of sustainable urbanization, UN, 2020. https://doi.org/10.18356/c41ab67e-en.
[2] U. Nations, Transforming our world: the 2030 Agenda for Sustainable Development, New York, USA, 2015. ⟨https://sdgs.un.org/2030agenda⟩.
[3] B.V.V. Reddy, Sustainable materials for low carbon buildings, Int. J. Low. -Carbon Technol. 4 (2009) 175–181, https://doi.org/10.1093/ijlct/ctp025.
[4] D. Gallipoli, A.W. Bruno, C. Perlot, J. Mendes, A geotechnical perspective of raw earth building, Acta Geotech. 12 (2017) 463–478, https://doi.org/10.1007/s11440-016-0521-1.
[5] G.H. Brundtland, The brundtland report: our common future, Med. War. (1987), https://doi.org/10.1080/07488008808408783.
[6] A. Hashemi, H. Cruickshank, A. Cheshmehzangi, Environmental impacts and embodied energy of construction methods and materials in low-income tropical housing, Sustainability 7 (2015) 7866–7883, https://doi.org/10.3390/su7067866.
[7] E. Mpakati-Gama, The use of alternative building materials in developing countries: addressing challenges faced by stakeholders, World Constr. Conf. (2012) 266–275.
[8] V. Rigassi, Compressed earth blocks. Volume I: manual of production, GATE (GTZ) (1995).
[9] H. Guillaud, T. Joffroy, P. Odul, Compressed Earth Blocks. Volume II: Manual of Design and Construction, GATE / GTZ (1995).
[10] P. Walker, T. Stace, Properties of some cement stabilised compressed earth blocks and mortars, Mater. Struct. Constr. 30 (1997) 545–551, https://doi.org/10.1007/bf02486398.

[11] E. Kathambi, K. Nille-Hauf, B. Fitik, J. Schänzlinn, Evaluating sustainable techniques for earthen wall construction- a qualitative study, J. Earth Environ. Sci. (2024), https://doi.org/10.47991/2835-7868/JEES.
[12] J.C. Morel, A. Mesbah, M. Oggero, P. Walker, Building houses with local materials: means to drastically reduce the environmental impact of construction, Build. Environ. 36 (2001) 1119–1126, https://doi.org/10.1016/S0360-1323(00)00054-8.
[13] V. Mora-Ruiz, J. Soto-Paz, S. Attia, C. Mejía-Parada, Sustainable earthen construction: a meta-analytical review of environmental, mechanical, and thermal performance, Page 918 15, Build 2025 15 (2025) 918, https://doi.org/10.3390/BUILDINGS15060918.
[14] M. Hall, Y. Djerbib, Rammed earth sample production: context, recommendations and consistency, Constr. Build. Mater. 18 (2004) 281–286, https://doi.org/10.1016/j.conbuildmat.2003.11.001.
[15] B.V.V. Reddy, P. Prasanna Kumar, Embodied energy in cement stabilised rammed earth walls, Energy Build. 42 (2010) 380–385, https://doi.org/10.1016/J.ENBUILD.2009.10.005.
[16] O.B. Adegun, Y.M.D. Adedeji, Review of economic and environmental benefits of earthen materials for housing in Africa, Front. Archit. Res. 6 (2017) 519–528, https://doi.org/10.1016/J.FOAR.2017.08.003.
[17] S. Boubekeur, V. Rigassi, Blocs de terre comprimée: procédures d'essais, 2000.
[18] C. Turco, A.C. Paula Junior, E.R. Teixeira, R. Mateus, Optimisation of Compressed Earth Blocks (CEBs) using natural origin materials: a systematic literature review, Constr. Build. Mater. 309 (2021) 125140, https://doi.org/10.1016/j.conbuildmat.2021.125140.
[19] B.V.V. Reddy, Compressed Earth Block & Rammed Earth Structures, Springer, 2022, https://doi.org/10.1007/978-981-16-7877-6.
[20] P. Lourenço, J. de Brito, F. Branco, The use of compacted earth blocks (BTC) in modern construction, in: O. Ural, V. Abrantes, A. Tadeu (Eds.), XXX IAHS World Congr. Hous., 2002: pp. 1–8.
[21] A. Shukla, G.N. Tiwari, M.S. Sodha, Embodied energy analysis of adobe house, Renew. Energy 34 (2009) 755–761, https://doi.org/10.1016/j.renene.2008.04.002.
[22] R.A. Bradley, M. Gohnert, Compressed stabilized earth block shell housing: performance considerations, Pract. Period. Struct. Des. Constr. 23 (2018) 1–18, https://doi.org/10.1061/(ASCE)SC.1943-5576.0000373.
[23] H. Niroumand, M.F.M. Zain, M. Jamil, A guideline for assessing of critical parameters on Earth architecture and Earth buildings as a sustainable architecture in various countries, Renew. Sustain. Energy Rev. 28 (2013) 130–165, https://doi.org/10.1016/j.rser.2013.07.020.
[24] G. Minke, Building with earth: design and technology of a sustainable architecture, BirkhäUse (2006).
[25] J.A. Bogas, M. Silva, M. da G. Gomes, Unstabilized and stabilized compressed earth blocks with partial incorporation of recycled aggregates, Int. J. Archit. Herit. (2018), https://doi.org/10.1080/15583058.2018.1442891.
[26] P. Walker, The Australian Earth Building Handbook (HB 195), Standards Australia, Sydney, 2002.
[27] A. Fabbri, J.C. Morel, J.E. Aubert, Q.B. Bui, D. Gallipoli, B.V.V. Reddy, Testing and characterisation of earth-based building materials and elements: State-of-the-Art Report of the RILEM TC 274-TCE (eds), Springer, Cham, 2022, https://doi.org/10.1007/978-3-030-83297-1_3.
[28] G.C. Bailly, Y. El Mendili, A. Konin, E. Khoury, Advancing earth-based construction: a comprehensive review of stabilization and reinforcement techniques for adobe and compressed earth blocks, Eng 5 (2024) 41, https://doi.org/10.3390/ENG5020041.
[29] J. López-Rebollo, X. Cárdenas-Haro, J.P. Parra-Vargas, K. Narváez-Berrezueta, J. Pino, Improvement of mechanical properties of compressed earth blocks with stabilising additives for self-build of sustainable housing, Buildings 14 (2024) 664, https://doi.org/10.3390/buildings14030664.
[30] M. Mostafa, N. Uddin, Experimental analysis of Compressed Earth Block (CEB) with banana fibers resisting flexural and compression forces, Case Stud. Constr. Mater. 5 (2016) 53–63, https://doi.org/10.1016/j.cscm.2016.07.001.
[31] P. Nshimiyimana, S. Omar Sore, C. Hema, O. Zoungrana, A. Messan, L. Courard, A discussion of optimisation of compressed earth blocks (CEBs) using natural origin materials: a systematic literature review, Constr. Build. Mater. 325 (2022) 1–21, https://doi.org/10.1016/j.conbuildmat.2022.126887.
[32] V. Rigassi, Compressed Earth Blocks. Volume I: Manual of Production, GATE / GTZ (1985).
[33] T.E. Elahi, A.R. Shahriar, M.S. Islam, Engineering characteristics of compressed earth blocks stabilized with cement and fly ash, Constr. Build. Mater. 277 (2021) 122367, https://doi.org/10.1016/J.CONBUILDMAT.2021.122367.
[34] B.V.V. Reddy, R. Lal, K.S.N. Rao, Influence of joint thickness and mortar-block elastic properties on the strength and stresses developed in soil-cement block masonry, J. Mater. Civ. Eng. 21 (2009) 535–542, https://doi.org/10.1061/(ASCE)0899-1561(2009)21:10(535).
[35] B.V.V. Reddy, Stabilised soil blocks for structural masonry in earth construction, in: M.R. Hall, R. Lindsay, M. Krayenhoff (Eds.), Mod. Earth Build. Mater. Eng. Constr. Appl, Woodhead Publishing Limited, Cambridge, UK, 2012, pp. 324–363, https://doi.org/10.1533/9780857096166.3.324.
[36] P. Dulal, S. Maharjan, M.P. Timalsina, Y. Maharjan, A. Giri, A. Tamang, Engineering properties of cement-stabilized compressed earth bricks, J. Build. Eng. 77 (2023) 107453, https://doi.org/10.1016/J.JOBE.2023.107453.
[37] C.T.S. Beckett, D. Ciancio, Durability of cement-stabilised rammed earth: a case study in Western Australia, Aust. J. Civ. Eng. 14 (2015) 1–9, https://doi.org/10.1080/14488353.2015.1092671.
[38] N. Sathiparan, R.A.N.S. Tharuka, P. Jeyananthan, Prediction of moisture content of cement-stabilized earth blocks using soil characteristics, cement content, and ultrasonic pulse velocity, J. Eng. Appl. Sci. 71 (2024) 187, https://doi.org/10.1186/S44147-024-00527-2.
[39] J.A. Bogas, S. Real, R. Cruz, B. Azevedo, Mechanical performance and shrinkage of compressed earth blocks stabilised with thermoactivated recycled cement, J. Build. Eng. 79 (2023) 107892, https://doi.org/10.1016/J.JOBE.2023.107892.
[40] A.T. Shiferaw, Carbon conscious construction: evaluating compressed stabilized earth blocks, Buildings 15 (2025) 4362, https://doi.org/10.3390/buildings15234362.
[41] B.V.V. Reddy, R. Lal, K.S. Nanjunda Rao, Optimum soil grading for the soil-cement blocks, J. Mater. Civ. Eng. 19 (2007) 139–148, https://doi.org/10.1061/(asce)0899-1561(2007)19:2(139).
[42] A.L. Murmu, A. Patel, Towards sustainable bricks production: an overview, Constr. Build. Mater. 165 (2018) 112–125, https://doi.org/10.1016/j.conbuildmat.2018.01.038.
[43] W. Powrie, Soil Mechanics: Concepts and Applications, 3rd ed, CRC Press, 2013, https://doi.org/10.1201/9781315275284.
[44] B.G. Richards, S. Peth, Modelling soil physical behaviour with particular reference to soil science, Soil Tillage Res 102 (2009) 216–224, https://doi.org/10.1016/j.still.2008.07.022.
[45] A. Vissac, L. Fontaine, R. Anger, Recettes traditionnelles & classification des stabilisants d'origine animale ou végétale, Grenoble, France, 2012.
[46] A. Fabbri, J.C. Morel, J.-E. Aubert, Q.-B. Bui, D. Gallipoli, A. Ventura, B.V. V. Reddy, A. Pelé-Peltier, H.N. Abhilash, An overview of the remaining challenges of the RILEM TC 274-TCE, testing and characterisation of earth-based building materials and elements, RILEM Tech. Lett. 6 (2021) 150–157, https://doi.org/10.21809/rilemtechlett.2021.149.
[47] G. Lan, S. Chao, Y. Wang, Y. Cui, Methods to Test the Compressive Strength of Earth Blocks, Adv. Mater. Sci. Eng. 2021 (2021) 1–11, https://doi.org/10.1155/2021/1767238.
[48] J. Yan, K. Yuan, F. Zhang, L. Guo, Study on mechanical properties and constitutive equation of earth materials under uniaxial compression, Appl. Sci. 13 (2022) 19, https://doi.org/10.3390/APP13010019.
[49] G. Lan, G. Weng, K. Zhang, Assessment of optimal specimen to measure the compressive strength of earthen-based masonry, Measurement 208 (2023) 112484, https://doi.org/10.1016/j.measurement.2023.112484.
[50] R. Bahar, M. Benazzoug, S. Kenai, Performance of compacted cement-stabilised soil, Cem. Concr. Compos 26 (2004) 811–820, https://doi.org/10.1016/J.CEMCONCOMP.2004.01.003.
[51] S. Diop, O.A. Sall, D. Diouf, M. Ba, Characterization of the influence of fly ash on the mechanical behavior of compressed earth bricks, Int. J. Res. Rev. 12 (2025) 107–114, https://doi.org/10.52403/ijrr.20250712.
[52] J. Taypondou Darman, J.H. Keyangue Tchouata, G.F. Ngôn Ngôn, F. Ngapgue, B. Lindou Ngakoupain, Y. Tchedele Langollo, Evaluation of lateritic soils of Mbé for use as compressed earth bricks (CEB), Heliyon 8 (2022), https://doi.org/10.1016/j.heliyon.2022.e10147.
[53] S.N. Malkanthi, A.A.D.A.J. Perera, Particle packing application for improvement in the properties of compressed stabilized earth blocks with reduced clay and silt, Eng. Technol. Appl. Sci. Res. 9 (2019) 4538–4542, https://doi.org/10.48084/etasr.3002.
[54] G. Santha Kumar, P.K. Saini, R. Deoliya, A.K. Mishra, S.K. Negi, Characterization of laterite soil and its use in construction applications: a review, Resour. Conserv. Recycl. Adv. 16 (2022) 200120, https://doi.org/10.1016/J.RCRADV.2022.200120.
[55] N.A. Wahab, M.J. Roshan, A.S.A. Rashid, M.A. Hezmi, S.N. Jusoh, N.D. N. Norsyahariati, S. Tamassoki, Strength and durability of cement-treated lateritic soil, Sustainability 13 (2021) 6430, https://doi.org/10.3390/SU13116430.
[56] W. Liu, H.B. Burato, J. Tan, X. Huang, F.S. Ackah, A review on improving the key engineering properties of lateritic soil by treating industrial by-products and wastes, Case Stud. Constr. Mater. 23 (2025) e04856, https://doi.org/10.1016/j.cscm.2025.e04856.
[57] B.V.V. Reddy, A. Gupta, Characteristics of soil-cement blocks using highly sandy soils, Mater. Struct. 38 (2005) 651–658, https://doi.org/10.1617/14265.
[58] B.B. Zewudie, Experimental study on the production and mechanical behavior of compressed lime-cement-stabilized interlock soil blocks, Adv. Mater. Sci. Eng. 2023 (2023), https://doi.org/10.1155/2023/2933398.
[59] Ahmed Bensaada, The impact of the use of cement as stabilizers on the mechanical and physical properties of compressed earth blocks: experiment design as a methodology, Power Syst. Technol. 49 (2025) 1056–1070, https://doi.org/10.52783/pst.1650.
[60] J.R. González-López, C.A. Juárez-Alvarado, B. Ayub-Francis, J.M. Mendoza-Rangel, Compaction effect on the compressive strength and durability of stabilized earth blocks, Constr. Build. Mater. 163 (2018) 179–188, https://doi.org/10.1016/j.conbuildmat.2017.12.074.
[61] A. Briga-Sá, R.A. Silva, N. Gaibor, V. Neiva, D. Leitão, T. Miranda, Mechanical characterization of masonry built with iCEBs of granite residual soils with cement–lime stabilization, Buildings 12 (2022), https://doi.org/10.3390/buildings12091419.
[62] T and D. AS, Historical Weather for Dakar in January 2024, (2026). ⟨https://www.timeanddate.com/weather/senegal/dakar/historic?month=1&year=2024⟩ (accessed April 14, 2026).
[63] J.C. Morel, A. Pkla, P. Walker, Compressive strength testing of compressed earth blocks, Constr. Build. Mater. 21 (2007) 303–309, https://doi.org/10.1016/j.conbuildmat.2005.08.021.

[64] UNI EN 12390-1: Testing hardened concrete - Part 1: Shape, dimensions and other requirements for specimens and moulds, (2021).
[65] UNI EN 12390-3: Testing hardened concrete - Part 3: Compressive strength of test specimens, (2019).
[66] P.J. Walker, Strength, durability and shrinkage characteristics of cement stabilised soil blocks, Cem. Concr. Compos 17 (1995) 301–310, https://doi.org/10.1016/0958-9465(95)00019-9.
[67] J.R. González-López, C.A. Juárez-Alvarado, B. Ayub-Francis, J.M. Mendoza-Rangel, Compaction effect on the compressive strength and durability of stabilized earth blocks, Constr. Build. Mater. 163 (2018) 179–188, https://doi.org/10.1016/j.conbuildmat.2017.12.074.
[68] H. Houben, P.E. Verney, Compressed Earth Blocks: Selection of Production Equipment, CDI, Brussels, 1989.
[69] J. Goutsaya, G.E. NTAMACK, B. Kenmeugne, S. Charif d'Ouazzane, Mechanical characteristics of compressed earth blocks, compressed stabilized earth blocks and stabilized adobe bricks with cement in the town of Ngaoundere - Cameroon, J. Build. Mater. Struct. 8 (2021) 139–159, https://doi.org/10.34118/jbms.v8i2.1441.
[70] J. Goutsaya, G.E. Ntamack, S.C. D'Ouazzane, Damage modelling of compressed earth blocks stabilised with cement, Adv. Civ. Eng. 2022 (2022), https://doi.org/10.1155/2022/3342661.
[71] E. Hall, B. Pulatsu, E. Erdogmus, B. Skourup, Compression, tension, and fracture energy properties of compressed cement-stabilized earth blocks, J. Archit. Eng. 28 (2022), https://doi.org/10.1061/(asce)ae.1943-5568.0000524.
[72] M. Mahdad, A. Benidir, A. Brara, Experimental assessment of mechanical behavior of a compressed stabilized earth blocks (CSEB) and walls, J. Mater. Eng. Struct. 8 (2021) 95–110.
[73] M.S. Islam, T.E. Elahi, A.R. Shahriar, N. Mumtaz, Effectiveness of fly ash and cement for compressed stabilized earth block construction, Constr. Build. Mater. 255 (2020) 119392, https://doi.org/10.1016/j.conbuildmat.2020.119392.
[74] T.E. Elahi, A.R. Shahriar, M.K. Alam, M.Z. Abedin, Effectiveness of saw dust ash and cement for fabrication of compressed stabilized earth blocks, Constr. Build. Mater. 259 (2020) 120568, https://doi.org/10.1016/j.conbuildmat.2020.120568.
[75] B. Taallah, A. Guettala, S. Guettala, A. Kriker, Mechanical properties and hygroscopicity behavior of compressed earth block filled by date palm fibers, Constr. Build. Mater. 59 (2014) 161–168, https://doi.org/10.1016/j.conbuildmat.2014.02.058.
[76] K.A. Heathcote, Durability of earthwall buildings, Constr. Build. Mater. 9 (1995) 185–189, https://doi.org/10.1016/0950-0618(95)00035-E.
[77] UNI EN 1015-11:2007: Methods of test for mortar for masonry - Part 11: Determination of flexural and compressive strength of hardened mortar, (2019).
[78] ASTM D6272-17: Standard Test Method for Flexural Properties of Unreinforced and Reinforced Plastics and Electrical Insulating Materials by Four-Point Bending, (2017).
[79] G. Macchi, Lezioni di tecnica delle costruzioni: allievi civili, CLUED, Milano, 1985.
[80] P. Fontana, L. Miccoli, U. Grünberg, Experimental investigations on the initial shear strength of masonry with earth mortars, Int. J. Mason. Res. Innov. 3 (2018) 34–49.
[81] C.B. de Carvalho Bello, A. Cecchi, Experiments on natural fibers: durability and mechanical properties, Adv. Mater. Process. Technol. 3 (2017) 632–639, https://doi.org/10.1080/2374068X.2017.1364880.
[82] R.D. Toledo Filho, K. Scrivener, G.L. England, K. Ghavami, Durability of alkali-sensitive sisal and coconut ® bres in cement mortar composites, Cem. Concr. Compos 22 (2000) 127–143, https://doi.org/10.1016/S0958-9465(99)00039-6.
[83] C.B. de Carvalho Bello, I. Boem, A. Cecchi, N. Gattesco, D.V. Oliveira, Experimental tests for the characterization of sisal fiber reinforced cementitious matrix for strengthening masonry structures, Constr. Build. Mater. 219 (2019) 44–55, https://doi.org/10.1016/j.conbuildmat.2019.05.168.
[84] A. Alqenaee, A. Memari, Experimental study of 3D printable cob mixtures, Constr. Build. Mater. 324 (2022) 126574, https://doi.org/10.1016/j.conbuildmat.2022.126574.
[85] W.F. Edris, H. Al-fhaid, M. Al-tamimi, Evolution of durability and mechanical behaviour of mud mortar stabilized with oil shale ash, lime, and cement, Civ. Eng. J. 9 (2023) 2175–2192, https://doi.org/10.28991/CEJ-2023-09-09-06©.
[86] D. Rocha, P. Faria, S.S. Lucas, Additive manufacturing of earth-based materials: a literature review on mortar composition, extrusion, and processing earth, Materials 17 (2024) 202, https://doi.org/10.3390/MA17010202.
[87] M. Pedergnana, S.T. Elias-ozkan, Impact of various sands and fibres on the physical and mechanical properties of earth mortars for plasters and renders, Constr. Build. Mater. 308 (2021) 125013, https://doi.org/10.1016/j.conbuildmat.2021.125013.
[88] T. Santos, M.I. Gomes, F. Coelho, P. Faria, Eco-efficient earth plasters: influence of clay content, sand particle size, and support, J. World Arch. 2 (2018) 1–12.
[89] K.L. Pickering, M.G.A. Efendy, T.M. Le, A review of recent developments in natural fibre composites and their mechanical performance, Compos. Part A 83 (2016) 98–112, https://doi.org/10.1016/j.compositesa.2015.08.038.
[90] B. Mazhoud, F. Collet, S. Pretot, C. Lanos, Mechanical properties of hemp-clay and hemp stabilized clay composites, Constr. Build. Mater. 155 (2017) 1126–1137, https://doi.org/10.1016/j.conbuildmat.2017.08.121.
[91] R. Paiva, A. Paiva, L. Caldas, O.A.M. Reales, R.D. Toledo Filho, Earth-based mortars: mix design, mechanical characterization and environmental performance assessment, Constr. Technol. Arch. 1 (2022) 271–278, https://doi.org/10.4028/www.scientific.net/CTA.1.271.
[92] T. Santos, M. Idália, A. Santos, E. Ferraz, P. Faria, Comparison of mineralogical, mechanical and hygroscopic characteristic of earthen, gypsum and cement-based plasters, Constr. Build. Mater. J. 254 (2020) 1–11, https://doi.org/10.1016/j.conbuildmat.2020.119222.
[93] N.P. Thatikonda, D. Baraldi, G. Boscato, A. Cecchi, Adaptation of DIC technique for simplified applications in experimental mechanics, J. Phys. Conf. Ser. 2802 (2024) 012008, https://doi.org/10.1088/1742-6596/2802/1/012008.
[94] N.P. Thatikonda, D. Baraldi, G. Boscato, A. Cecchi, DIC technique for experimental validation of higher order numerical models, J. Phys. Conf. Ser. 2698 (2024) 012022, https://doi.org/10.1088/1742-6596/2698/1/012022.
[95] M. Benzerara, R. Belouettar, A. Perrot, M. Geomaterials, Combined and synergic effect of algerian natural fibres and biopolymers on the reinforcement of extruded raw earth, Constr. Build. Mater. 289 (2021) 123211 https://doi.org//10.1016/j.conbuildmat.2021.123211.
[96] G. Silva, R. Nanez, Z. Diana, V. Burgos, S. Kim, G. Ruiz, M.A. Pando, A. Rafael, J. Nakamatsu, Eco-friendly additive construction: analysis of the printability of earthen-based matrices stabilized with potato starch gel and sisal fibers, Constr. Build. Mater. 347 (2022) 128556, https://doi.org/10.1016/j.conbuildmat.2022.128556.
[97] UNI EN 1052-1:2001: Methods of test for masonry - Part 1: Determination of compressive strength, (2001).
[98] T.P. Bhatt, Compressive strength characteristics of compressed stabilized earth block (CSEB) units and walls, J. Eng. Technol. Plan 5 (2024) 61–70, https://doi.org/10.3126/joetp.v5i1.69647.
[99] L. Miccoli, A. Garofano, P. Fontana, U. Müller, Experimental testing and finite element modelling of earth block masonry, Eng. Struct. 104 (2015) 80–94, https://doi.org/10.1016/j.engstruct.2015.09.020.
[100] K. Al-Jabri, A.W. Hago, S. Al-Saadi, P. Amoatey, I. Al-Harthy, Structural and thermal performance of sustainable interlocking compressed earth blocks masonry units made with produced water from oilfields, Case Stud. Constr. Mater. 17 (2022) e01186, https://doi.org/10.1016/j.cscm.2022.e01186.
[101] I. Kafodya, F. Okonta, P. Kloukinas, Role of fiber inclusion in adobe masonry construction, J. Build. Eng. 26 (2019) 100904, https://doi.org/10.1016/j.jobe.2019.100904.
[102] N.N. Thaickavil, J. Thomas, Behaviour and strength assessment of masonry prisms, Case Stud. Constr. Mater. 8 (2018) 23–38, https://doi.org/10.1016/j.cscm.2017.12.007.
[103] A. Anthoine, Derivation of the in-plane elastic characteristics of masonry through homogenization theory, Int. J. Solids Struct. 32 (1995) 137–163, https://doi.org/10.1016/0020-7683(94)00140-R.
[104] A. Cecchi, R. Di Marco, Homogenization of masonry walls with a computational oriented procedure. Rigid or elastic block? Eur. J. Mech. A/Solids 19 (2000) 535–546, https://doi.org/10.1016/S0997-7538(00)00159-5.
[105] A. Cecchi, K. Sab, A multi-parameter homogenization study for modeling elastic masonry, Eur. J. Mech. A/Solids 21 (2002) 249–268, https://doi.org/10.1016/S0997-7538(01)01195-0.
[106] D. Baraldi, A. Cecchi, A. Tralli, Continuous and discrete models for masonry like material: a critical comparative study, Eur. J. Mech. A/Solids 50 (2015) 39–58, https://doi.org/10.1016/j.euromechsol.2014.10.007.
[107] A. Cecchi, K. Sab, Out of plane model for heterogeneous periodic materials: the case of masonry, Eur. J. Mech. A/Solids 21 (2002) 715–746, https://doi.org/10.1016/S0997-7538(02)01243-3.